Adaptive Control of Time Delay Systems and Applications to Automotive Control Problems

by

Yildiray Yildiz

Submitted to the Department of Mechanical Engineering
in partial fulfillment of the requirements for the degree of

Doctor of Philosophy in Mechanical Engineering

at the

MASSACHUSETTS INSTITUTE OF TECHNOLOGY

February 2009

Author .....
Department of Mechanical Engineering
January 26, 2009

Certified by .....
Anuradha Annaswamy
Senior Research Scientist
Thesis Supervisor

Accepted by .....
David Hardt
Chairman, Department Committee on Graduate Theses

Adaptive Control of Time Delay Systems and Applications to Automotive Control Problems

by

Yildiray Yildiz

Submitted to the Department of Mechanical Engineering
on January 26, 2009, in partial fulfillment of the
requirements for the degree of
Doctor of Philosophy in Mechanical Engineering

Abstract

This thesis is about the adaptive control of time delay systems with applications to automotive control problems. The stabilization of systems involving time delays is a difficult problem since the existence of a delay may induce instability or poor performance for the closed loop system. A unique approach for controlling systems with known time delay was originated by Otto Smith in the 1950s by compensating for the delayed output using input values stored over a time window of $[t-\tau, t]$ and estimating the plant output using a model of the plant. Later, this idea was extended to include unstable plants as well, using finite-time integrals of the delayed input values thereby avoiding unstable pole-zero cancellations that may occur in Smith's controller. Adaptive versions of these delay compensating controllers were also developed with rather complicated adaptive rules which might not be practical to use in real applications. In this thesis, a simpler adaptive version of delay compensating controllers is developed, which has adaptive rules that are easily implementable and thus suitable for real life implementations. The developed controller is tested in two important automotive control problems that are idle speed control (ISC) and fuel-to-air ratio (FAR) control. These two applications, ISC and FAR control, constitute the experimental part of this research.

In ISC, the objective is to regulate the engine speed to a prescribed set-point in the presence of accessory load torque disturbances such as due to air conditioning and power steering. The adaptive controller, integrated with the existing proportional spark controller, is used to drive the electronic throttle actuator. Both simulation and experimental results demonstrating the performance improvement by employing the adaptive controller are presented. Modifications and improvements to the controller structure, which were developed during the course of experimentation to solve specific problems, are also presented. In addition, the potential for the reduction in calibration time and effort which can be achieved with our approach is discussed.

The objective in FAR control is to maintain the in-cylinder FAR at a prescribed set point, determined primarily by the state of the Three-Way Catalyst (TWC), so that the pollutants in the exhaust are removed with the highest efficiency. The FAR

controller must also reject disturbances due to canister vapor purge and inaccuracies in air charge estimation and wall-wetting (WW) compensation. Two adaptive controller designs are considered. The first design is based on feedforward adaptation while the second design is based on both feedback and feedforward adaptation. Both simulation and experimental results demonstrating the performance improvement by employing the APC are presented. In addition, modifications and improvements to the APC structure, which were developed during the course of the experiments, to solve specific implementation problems are presented.

Thesis Supervisor: Anuradha Annaswamy
Title: Senior Research Scientist

Acknowledgments

Dr. Anuradha Annaswamy. You may not know, but when I first come to your office to express my interest in your work, I had little hope that you would offer me a research assistant position. I was very interested in controls but I was about to turn back home with all my dreams in my bag, due to lack of funding. You are the one who enabled me to follow my dreams, stay at MIT, conduct great research, complete this thesis and, finally, pursue my passion by getting an offer from NASA for my postdoctoral studies. Thank you.

Dr. Ilya Kolmanovsky. Your encouragement during tough times and your motivation during good times provided me enough fuel to complete this research. Your comments like "Great work!" have always made me feel that I'm responsible to really deserve these words. Thank you for always supporting me.

Dr. Diana Yanakiev. After the first few days that I spent with you, it was clear to me that you would not accept anything less than my best from me. I believe that I was very lucky to work with a mentor who was as demanding as you, always focused and always honest and critical, in a good way, to my work. Thank you.

Professor Kamal Youcef-Toumi and Professor Ahmed F. Ghoniem. I would like to thank you for serving as my committee members although you have a very busy schedule. You always made me think about the important points that I was otherwise not considering and you played a critical role in making this research as rigorous as possible.

Professor Mustafa Unel. Again, thank you for your support, encouragement, motivation, teaching and coaching. Most importantly, thank you for always trusting me.

Dr. Davor Hrovat of Ford Motor Company. Thank you for your support and encouragement. Chris Teslak and Steve Magner of Ford Motor Company. Thank you for your help with the experimental setup and for valuable discussions.

My labmates Dr. Jinho Jang, Travis Gibson, Zachary T. Dydek, Manohar Srikanth and Megumi Matsutani. Thank you for providing a cozy and enjoyable studying en-

vironment, and thank you for your friendship.

Dr. Zekeriyya Gemici. Thank you for being my friend and for challenging me on almost all subjects we can find to talk about. You are among the few people that I resonate with the same frequency. And of course, thank you for your contribution of 10 pounds to my body weight after all those sundae sessions.

Tugba Uzer. You are my inspiration and my passion. Thank you for your existence.

My whole family. Tugba, thank you for being a wonderful sister. Abutel Hala and Gulderen Hala, thank you for your unconditional love and support. Nene, thank you for your prayers. Mom and dad, thank you for being great parents. Thank you for your constant encouragement and support and love. I'm very lucky to be a member of this big family.

Thank you Ford Motor Company, for generously supporting this research.

Contents

1 Introduction **13**

1.1 Adaptive Posicast Control (APC) 13

1.2 Idle Speed Control (ISC) 15

1.3 Fuel-to-Air Ratio (FAR) Control 18

2 Adaptive Posicast Control Theory **23**

2.1 First-Order Plant 23

2.1.1 The Posicast Controller 24

2.1.2 The Adaptive Posicast Controller 25

2.2 State variables accessible 27

2.3 Adaptive Posicast Control in the presence of input-output measurements with $n^* \leqslant 2$ 28

2.3.1 Exact model matching for delayed systems 29

2.3.2 Adaptive Controller 32

2.3.3 Stability Analysis 36

2.3.4 Possible Nonlinear Extention 45

2.4 Summary 47

3 Spark Ignition Engine Idle Speed Control: An Adaptive Control Approach **49**

3.1 Plant Model 49

3.1.1 Throttle Mass Flow 49

3.1.2 Intake Manifold 50

3.1.3 Engine Air Mass Flow 50
3.1.4 Torque Generation 51
3.1.5 Engine Rotational Dynamics 51
3.1.6 Final Model for ISC 51
3.2 APC Design 53
3.2.1 Initial Design 53
3.2.2 Implementation Enhancements 56
3.2.3 Final Design and Calibration 61
3.3 Simulations 62
3.4 Experiments 63
3.4.1 Set-point Tracking 64
3.4.2 Disturbance Rejection 65
3.4.3 Robustness 66
3.5 Summary 67

4 Spark Ignition Engine Fuel-to-Air Ratio Control: An Adaptive Control Approach 71
4.1 Plant Model 71
4.1.1 Wall-Wetting (WW) Dynamics 72
4.1.2 FAR Formation and Propagation to the UEGO Sensor 73
4.1.3 Sensor Dynamics 73
4.1.4 Reduced Order Model 74
4.2 Controller Design 74
4.2.1 Baseline Controller 75
4.2.2 Adaptive Feedforward Controller (AFFC) 76
4.2.3 Adaptive Posicast Controller (APC) 78
4.2.4 Implementation Enhancements 78
4.2.5 Final Design and Calibration 83
4.3 Simulation and Experimental Results 84
4.3.1 AFFC vs. Baseline Controller 85

4.3.2 APC vs. Baseline Controller 87
4.3.3 APC vs. Gain-Scheduled Smith Predictor 92
4.4 Summary 94

5 Summary and Future Research **97**

A The Bound on the Series S **101**

B Disturbance Rejection Proof **103**

C Memory Requirements and Computational Complexity **105**

D Stability of Integral Approximation **107**

List of Figures

1-1 TWC efficiency vs. air-to-fuel ratio. 19

2-1 Exact model matching, Controller NC. 30

2-2 Exact model matching, Controller C. 32

3-1 Bode plots of $G(s)$ and $G_0(s)$ 52

3-2 Nonlinear model set-point tracking. Adaptation rates are calculated using (3.27) with no further tuning. 63

3-3 Nonlinear model set-point tracking. $z_u = z_r = 1$, $z_y = 220$. 63

3-4 Rapid prototyping with MicroAutoBox using CAN. 64

3-5 Comparison of the baseline controller with adaptive controller for set-point tracking. Γ_w is the same used in the simulation shown in Fig. 3-3 65

3-6 Comparison of the baseline controller with adaptive controller for power steering disturbance rejection at 650 rpm. Γ_w is the same used in the simulation shown in Fig. 3-3 66

3-7 Comparison of the baseline controller with adaptive controller for power steering disturbance rejection at 900 rpm. Γ_w is the same used in the simulation shown in Fig. 3-3 66

3-8 Comparison of the baseline controller with adaptive controller for power steering disturbance rejection at 590 rpm. Γ_w is the same used in the simulation shown in Fig. 3-3 67

3-9 Top figure: Adaptive controller performance for power steering disturbance. Bottom figure: Evolution of the controller parameters. 68

3-10 Top figure: Adaptive controller performance for power steering disturbance. Bottom figure: Evolution of the controller parameters with σ-modification. 68

4-1 Plant block diagram representation. 72
4-2 Overall closed loop controller structure. 75
4-3 Inner-loop structure with AFFC. 77
4-4 Rapid prototyping with MicroAutobox using CAN. 84
4-5 Comparison of baseline controller and AFFC. a) Response to a set-point change b) Response to purge disturbance. 86
4-6 Baseline controller vs. AFFC a) Φ and air flow rate when baseline controller is active b) Φ and air flow rate when AFFC is active c) Engine speeds d) Purge fuel flow rates. 88
4-7 Comparison of baseline controller with APC for purge disturbance rejection at 700 rpm. 89
4-8 Comparison of baseline controller with APC for purge disturbance rejection at 1000 rpm, with $c = 1$. 89
4-9 Time histories of a) Φ, b) Engine speed c) Engine relative air flow, d) Tracking error integral, during vehicle acceleration and deceleration for APC vs. baseline controller, with $c = 1$. 90
4-10 Comparison of baseline controller with APC during vehicle acceleration, with $c = 1.5$. 91
4-11 Time histories of a) Φ b) Engine relative air flow c) Feedback control input d) Tracking error integral, during vehicle acceleration and deceleration for gain-scheduled SP vs. APC, with $c = 1.5$. 93
4-12 Comparison of SP and APC for input step disturbance rejection in the presence of sensor time constant uncertainty. 95
4-13 Comparison of SP and APC for input step disturbance rejection in the presence of sensor time constant and delay uncertainty. 95

Chapter 1

Introduction

1.1 Adaptive Posicast Control (APC)

A time delay can be defined as the time interval from the application of a control signal to any observable change in the measured variable [1]. Time delays are ubiquitous in dynamical systems, present as computational delays, input delays, measurement delays and transportation/convection lags to name a few. In addition, higher order dynamical systems can often be modeled by low order systems plus a time delay. Many examples of systems including time delays, such as chemical, biological, mechanical, physiological and electrical systems, are given in [2] and [3]. Detailed surveys of time delay systems can be found in [4] and [5].

The stabilization of systems involving time delays is a difficult problem since the existence of a delay may induce instability or bad performance for the closed loop system. In many controller designs, the delay is neglected and stability and robustness margins are given with respect to delay. The same approach can also be found in some adaptive control designs [6]. However, in general, these approaches produces small delay margins.

A unique approach, called the Smith Predictor (SP), was originated by Otto Smith in the 1950s to solve the problem of controlling the systems with large delays [7]. The main idea in this approach is predicting the future output of the plant, using a plant model, and using this prediction to cancel the effect of the time delay. This

future prediction inspired the name for the "posi-cast", which stands for "positively (fore)casting". This is different from the feedforward control technique, also known as posicast control, used to cancel the oscillatory behavior of lightly damped systems. See also [8], [9], [10] and [11] for improvements and modifications on SP ideas. SP method, however, is not suitable for unstable systems due to the possibility of unstable pole-zero cancellations. A method, called finite spectrum assignment (FSA), that works also for unstable systems was introduced by Manitius and Olbrot, where the main contribution was using finite time integrals to prevent unstable pole zero cancellations [12]. See also [13], [14] and [15] for FAS techniques. An analogous solution in frequency domain is given by Ichikawa in [16]. Although these approaches solve the problem of controlling time delay systems, their success depends on accurate plant models. In reality, it is not easy to obtain reliable plant models and, in general, the plant parameters contain a degree of uncertainty. In addition, these parameters may change over time. Addressing this problem, in [17], Ortega and Lozano introduced an adaptive version of these delay compensating controllers using an augmented error approach [18]. Although this controller introduces adaptation and removes the need for accurate plant models, it has high complexity. A simple controller is generally more advantageous if it is meant to be used in industrial applications, especially in mass production implementations. In addition, the plant poles are restricted to multiplicity one in this controller. In [19], a simpler adaptive design, called Adaptive Posicast Controller (APC) is given with the same plant pole restriction. In this thesis, a rigorous treatment of the APC is given without any restrictions on plant pole multiplicities, and carefully addressing the necessary technical details.

As mentioned above, the APC is suitable for industrial applications due to its simplicity and low computational requirement. These features are important especially in the mass production applications such as automotive engine control. Triggered by the governmental regulations on emissions in 1960's and 1970's, the introduction of the microprocessor-based control permitted the automotive manufacturers to design cleaner, more fuel efficient, better performing and more reliable powertrain systems. The associated control problems provide continuing challenges to control engineers as

the requirements progressively become more stringent. Higher levels of performance and robustness are expected, while the calibration time and effort need to be reduced. Advances in control theory can be exploited to address these challenges. See [20] for an introduction to modeling and control of internal combustion engines.

In this research, we applied the APC to two important automotive control problems: the idle speed control (ISC) problem and the fuel-to-air ratio (FAR) control problem. In both of these applications, the APC performed better than the baseline controllers that are existing in the test vehicles. These two control problems are explained in detail below.

1.2 Idle Speed Control (ISC)

The basic problem of Idle Speed Control (ISC) is to maintain the engine speed at a prescribed set-point in the presence of various disturbances such as due to air conditioning, transmission engagement or power steering accessory load torques [21]. There are several well-known challenges in this control problem, one of the most important of which is the time-delay between the intake event and combustion event of the engine. This time delay limits the achievable performance in the electronic throttle control loop. The second challenge is that the controller performance must be robust to changes in the idle speed set-point, to changes in operating conditions (varying altitude, engine temperature and/or ambient temperature, etc.) and to part-to-part and aging-caused variability. Finally, obtaining an accurate and simple model which is appropriate for control design can be both difficult and time-consuming.

Idle Speed Control has been a classical problem in automotive control, and the celebrated Watt's governor (1796) was, in fact, a speed controller for a steam engine. Even though ISC is implemented in most of the vehicles on the road today, increasingly stringent regulatory and customer requirements necessitate its continuing improvement. For instance, a better performing ISC can improve fuel economy by reducing spark reserve and lowering idle speed set-point, and it can also accommodate changes in sensors and actuators (e.g., a replacement of an air-bypass-valve by the

electronic throttle or reduction in sensor or actuator cost). Finally, ISC designs that can lower calibration time and effort can help reduce time-to-market, which is a key priority for automotive manufacturers.

The ISC problem is typically addressed by combining some form of a feed-forward control with a closed-loop compensation based on the engine speed error. The feed-forward controller may consist of multiple look-up tables which may, for instance, predict the loads due to accessories for different operating conditions. A closed-loop controller determines the compensation with electronic throttle and spark timing actuators for the engine speed tracking error and is typically gain-scheduled on operating conditions where nonlinear maps may be used to determine the gains. The major effort in the calibration, which is the process of tuning control system parameters, is spent in determining the gains of the feed-forward controller. One of the reasons for this may be due to the low capability of the closed loop controller, which in turn shifts the burden of compensation to the feed-forward controller.

Many different closed loop designs have been proposed in the literature including $\mathcal{H}_\infty$ control [22], $\mathcal{H}_2$ control [23], sliding mode control [24], [25], ℓ_1 optimization [26], feedback linearization [27], proportional-integral (PI) and proportional-integral-derivative (PID) control [28], [29], [30], [31], [32], linear quadratic control (LQ) [33], [31], [34], model predictive control (MPC) [35], adaptive control [36], [37], [38] and estimation based control [39], [40], [41], to name a few. A comparison between different control algorithms for the idle speed control problem can be found in [42]. A comprehensive survey of engine models and control strategies developed for ISC can be found in [21].

The literature, given above, about classical and advanced control applications to the ISC problem, proves the continuing interest in an automated, model based control approach, and our work built upon these results by eliminating the need of a precise engine model for classical or optimization based algorithms and by reducing the conservatism introduced by the robust control approaches. This is achieved by using the Adaptive Posicast Controller (APC) developed in this thesis [19], [43], which is an adaptive controller for time delay systems. Successful adaptive control approaches

are presented also in references [36], [37], [38], but our approach is different from these: In [36], the adaptation is used to select the idle speed set point and in [37], the torque differences among the cylinders are estimated to reduce the short term fluctuations caused by them. Finally, in [38], simulation results of idle speed control by online estimation of the plant parameters and using these estimates in the control scheme using two actuators, spark and bypass valve, are given. In our approach, we apply the APC, a model reference adaptive controller developed for time delay systems, to control the idle speed at a prescribed set-point, in the presence of external disturbances, like power steering disturbance, and uncertainties due to modeling inaccuracies and operating point changes. We do not employ an online parameter estimation algorithm which may require additional computation power. In addition, we present experimental results demonstrating the improvements of the algorithm over the baseline controller existing in the vehicle, as well as the robustness of the algorithm by showing the parameter evolution during the course of the experiment.

The APC approach addresses the key challenges due to uncertainties and time delay that are important for ISC application. The underlying control architecture includes several components including the classical Smith Predictor [7], its variant reported in [12] based on finite-spectrum assignment, and adaptation [16], [17]. The controller is modified from its original design to take care of the specific needs of the idle speed control application and additional design methods are developed to facilitate the controller deployment: Firstly, an algorithm is developed for the adaptation rate selection. Secondly, a fine-tuning method is introduced to minimize the controller tuning. Finally, a robustifying scheme is used to prevent the drift of the adaptive parameters. Our main contribution is the demonstration of the potential of this adaptive controller to improve the performance and to reduce the time and effort required for the controller calibration. This is achieved by the help of modifications and improvements that are listed above.

The experimental results obtained using Ford F-150 test vehicle demonstrate the capability of the controller to improve performance and decrease the calibration time and effort.

Adaptive Posicast ISC approach represents a step towards a fully self-calibrating ISC because less reliance on feed-forward characterization of accessory loads is required, and because the controller gains are automatically tuned online.

While our control approach is adaptive, its development both benefits from and depends on the structural properties of the underlying plant model. This plant model for ISC control is briefly discussed in Chapter 3, while the reader is referred to [20] for a more extended treatment of the underling modeling techniques.

1.3 Fuel-to-Air Ratio (FAR) Control

The Fuel-to-Air Ratio (FAR) control is one of the most important control problems for conventional gasoline engines. The FAR control performance can strongly impact key vehicle attributes such as emissions, fuel economy and drivability. For instance, the FAR in engine cylinders must be controlled in such a way that the resulting exhaust gases can be efficiently converted by the Three-Way Catalyst (TWC). The TWC efficiency is about 98 percent when the fuel is matched to air charge in exactly stoichiometric proportion and drops abruptly outside a narrow region as seen in Fig. 1-1 [44]. The TWC can also compensate for the temporary FAR deviation from stoichiometry, by either storing excess oxygen or releasing oxygen to convert oxides of nitrogen (NO_x), excess hydro-carbons (HC) and carbon monoxide (CO). Thus, for the TWC to operate efficiently, the stored oxygen level must be regulated so that a range to accommodate further release or storage during transient conditions is available [20]. The oxygen storage level in the TWC may be inferred on the basis of the TWC model and a signal from a switching Heated Exhaust Gas Oxygen (HEGO) sensor located downstream of the TWC. In addition, the oxygen storage capacity of the TWC depends on the size and precious metal loading of the TWC. Therefore, if the FAR excursions and their durations are reduced with a well-performing controller, the storage capacity of TWC and its cost may be reduced as well.

A conventional FAR control system includes two nested controllers. The outer-loop controller generates a reference FAR (set-point) for the inner-loop controller

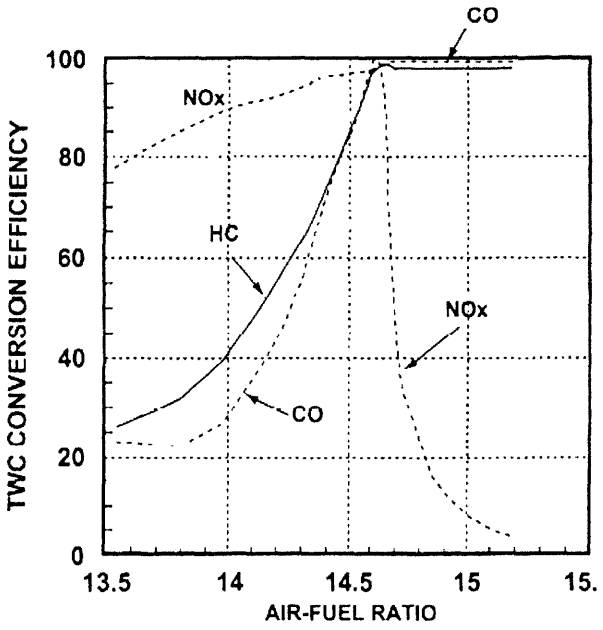

Figure 1-1: TWC efficiency vs. air-to-fuel ratio.

based, for instance, on the deviation of the estimated TWC stored oxygen state. The inner-loop controller maintains the FAR upstream of the TWC at this set-point by using the measurements of the feedgas FAR with a linear Universal Exhaust Gas Oxygen (UEGO) sensor to appropriately correct engine fueling rate. Small amplitude low frequency periodic modulation may be superimposed over the set-point to further improve catalyst efficiency. The HEGO sensor downstream of the TWC is also used to improve robustness to UEGO sensor drifts, changes to fuel type, and for diagnostics.

The inner loop controller consists of a feedforward component which is fast but may not be always accurate, and a feedback component which is slower but eliminates the steady-state error [20]. The feedforward component consists of estimation of the air and fuel path dynamics combined with appropriate compensations. These air and fuel dynamics correspond, mainly, to the intake manifold lag that affects the air charge, and the wall-wetting (WW) that determines the amount of fuel inducted into the cylinder for each fuel injection event during transient operation.

The FAR control problem has been extensively investigated over many years. In terms of advanced approaches, here we mention the use of nonlinear feedforward

controllers [45], adaptive controllers [46], [47], [48], [49], feedback linearization [50], observer based controllers [51], [52], [53], sliding mode controllers [54], [55], [56], linear quadratic regulators [57], [58], H_∞ controllers [59], [60], Smith Predictors [61], neural network controllers [62] and model predictive controllers [63]. The use of an electronic throttle as an additional control actuator [64] or secondary/port throttles [65] has also been explored. Apart from stoichiometric FAR controllers, reference [66] considers control of FAR in a lean burn engine using linear parameter-varying controllers. In addition to these, reference [67] presents an interesting example of estimating the FAR in the cylinders without using the oxygen sensor and thus reducing the time delay in the system, and [68] considers estimating the fuel-film dynamics. The motivation for these and related studies has been to achieve improved performance and robustness of the FAR control thereby enabling emission, fuel economy and drivability improvements.

Main challenges in the design of the FAR controller include variable time delay, uncertain plant behavior and disturbances. The time delay in the system comprises two basic components [66]: the time it takes from the fuel injection calculation to exhaust gas exiting the cylinders and the time it takes for the exhaust gases to reach the UEGO sensor location. The time delay in the system is a key factor limiting the bandwidth of the FAR feedback loop. The plant uncertainties are the result of inaccuracies in the air charge estimation and in the WW compensation, as well as changes in the UEGO sensor due to aging. When the carbon canister, which stores the fuel vapor generated in the fuel tank, is purged, the fuel content in the purge flow into the intake manifold is also uncertain and creates disturbance to the FAR control loop.

We, therefore, are interested in a control approach which can handle both uncertainties and large time-delays, and that can achieve high performance. The literature, given above, about classical and advanced control applications to the FAR control problem demonstrates continuous interest in an automated, model based control approach, and our work is built upon these results by eliminating the need of a precise engine model for classical or optimization based algorithms and by reducing the con-

servatism introduced by the robust control approaches. This is achieved by using the Adaptive Posicast Controller (APC) [19], [43], which is an adaptive controller for time delay systems. Successful adaptive control approaches are presented also in references [46], [47], [48] and [49], but our approach is different from them: In [46] and [48], a nonlinear least squares parameter identification method is used to identify the plant parameter values online and then these values are used in the controller. For the convergence of these parameters, the condition of persistent excitation is needed. In addition, this online parameter identification may require extra computational power. In both of the references, the controllers are applied to a single cylinder laboratory engine. In [47], again a similar approach is taken where an extended Kalman Filter is used to identify the plant parameter values online. Similarly, in [49], the authors use a step by step experimental procedure to identify the sensor time constant, during the time of operation, where a rich input excitation is needed for parameter convergence. Our approach is based on direct adaptation where an online parameter identification scheme is not used. In addition, we apply the APC to a Lincoln Navigator test vehicle with 8 cylinders, which makes the control task much harder due to cylinder to cylinder and bank-to-bank variations. Finally, in our work, we do not only present our results but also give a comparison with the existing control design in the test vehicle and with a gain scheduled Smith Predictor.

The Adaptive Posicast Control (APC) is a recently developed control design approach that is especially suited for plants with large time-delays [19], [43] and parametric uncertainties. The APC can be described as an adaptive controller that combines explicit delay compensation, using the classical Smith Predictor [7] and finite spectrum assignment [12], and adaptation [16], [17]. Due to such a unique combination, the APC effectively deals with both uncertainties and large time-delays both of which are dominant features of the FAR control problem.

To fit the specific needs of the FAR application, our design has been extended with additional features: First, an adaptive feedforward term is added which is crucial for disturbance rejection. Second, procedures are developed for the controller parameter initialization and the adaptation rate selection to reduce the calibration time and

effort. Third, an algorithm to take care of the variable delay is introduced. Fourth, an anti-windup logic is used to prevent the winding up the integrators used for parameter adaptation. Finally, a robustifying scheme is used to prevent the drift of the adaptive parameters. Our main contribution is the demonstration of the potential of this adaptive controller to improve the performance and to reduce the time and effort required for the controller calibration. This is achieved by the help of modifications and improvements that are listed above.

The experimental results were obtained using a Lincoln Navigator test vehicle provided by Ford Motor Company, Dearborn, USA. These results indicate the capability of the controller to improve performance and decrease the calibration time and effort.

Adaptive Posicast FAR control approach represents a step towards a fully self-calibrating FAR controller because it reduces reliance on feedforward characterization and because the controller gains are automatically tuned online.

For comparison with the APC, we also develop, in this thesis, a feedforward adaptive controller that attempts to minimize the impact of the purge fuel disturbance. We also compare this controller with the baseline controller using simulations and in-vehicle experiments.

The plant model for FAR ratio control is briefly discussed in Chapter 4, while the reader is referred to [20] for a more extended treatment of the underlying modeling techniques.

Chapter 2

Adaptive Posicast Control Theory

2.1 First-Order Plant

We begin with a simple problem, where the plant is given by

$$\dot{x}(t) = ax(t) + u(t) \tag{2.1}$$

for which a control input of the form

$$u(t) = \theta^* x(t) + r(t) \qquad \theta^* = a_{\mathrm{m}} - a, \quad a_{\mathrm{m}} < 0 \tag{2.2}$$

ensures stable tracking for any a. One can provide a more formal guarantee of such a tracking by choosing a reference model of the form

$$\dot{x}_{\mathrm{m}}(t) = a_{\mathrm{m}} x_{\mathrm{m}}(t) + r(t) \tag{2.3}$$

which leads to error dynamics of the form

$$\dot{e}(t) = a_{\mathrm{m}} e(t) \qquad e(t) = x(t) - x_{\mathrm{m}}(t) \tag{2.4}$$

for which it can be simply shown that $V(t) = \frac{1}{2}e^2(t)$ is a Lyapunov function, with $\dot{V} < 0$, leading to exponential stability.

2.1.1 The Posicast Controller

We now introduce a time delay in (2.1) so that

$$\dot{x}(t) = ax(t) + u(t - \tau) \tag{2.5}$$

where the goal is to stabilize the plant and track the output of a stable reference model. The results of [7] and [12] inspire us to establish the following: A posicast controller that "positively" forecasts the output is chosen as

$$u(t) = \theta^* x(t + \tau) + r(t) \tag{2.6}$$

which in turn leads to a closed-loop system of the form

$$\dot{x}(t) = a_{\mathrm{m}} x(t) + r(t - \tau), \tag{2.7}$$

an obviously stable plant. The non-causal controller in (2.6) can be shown to be indeed causal with a clever algebraic manipulation established in [12]. This is enabled by observing that the plant equation in (2.5) can be written in an integral form as

$$x(t + \tau) = e^{a\tau} x(t) + \int_{-\tau}^{0} e^{-a\eta} u(t + \eta) d\eta. \tag{2.8}$$

The above observation also leads us to a PosiCast Lyapunov function for the closed-loop system given by (2.5)-(2.6), for the case when $r(t) = 0$, given by

$$V(t) = \frac{1}{2} x^2(t + \tau). \tag{2.9}$$

It can be shown from (2.8) and some algebra that

$$\dot{V}(t) = a_{\mathrm{m}} x^2(t + \tau). \tag{2.10}$$

2.1.2 The Adaptive Posicast Controller

We now proceed to the case when a is unknown. Using customary adaptive control procedures [18], suppose we choose a control input of the form

$$u(t) = \theta x(t+\tau) + r(t) \tag{2.11}$$

it leads to a closed-loop system of the form

$$\begin{aligned} \dot{x}(t) &= a_{\mathrm{m}} x(t) + \tilde{\theta}(t-\tau)\left[e^{a\tau}x(t-\tau) + \int_{-\tau}^{0} e^{-a\eta}u(t+\eta-\tau)d\eta\right] \\ &\quad + r(t-\tau) \end{aligned} \tag{2.12}$$

where $\tilde{\theta}(t) = \theta(t) - \theta^*$. While indeed this suggests that a reference model can be chosen in the form

$$\dot{x}_{\mathrm{m}}(t) = a_{\mathrm{m}} x_{\mathrm{m}}(t) + r(t-\tau), \tag{2.13}$$

it can be seen that it poses a difficulty, since the underlying error model can be derived using (2.12) and (2.13) as

$$\dot{e}(t) = a_{\mathrm{m}} e(t) + \tilde{\theta}(t-\tau)\left[e^{a\tau}x(t-\tau) + \int_{-\tau}^{0} e^{-a\eta}u(t+\eta-\tau)d\eta\right]. \tag{2.14}$$

Equation (2.14) is however not in a form that lends itself to a Lyapunov function since the term inside the brackets includes the unknown parameter a. We therefore choose a different control input that is still motivated by the non-adaptive controller given in (2.6).

Equations (2.6) and (2.8) imply that the Posicast control input is essentially of the form

$$u(t) = \theta_{\mathrm{x}}^* x(t) + \int_{-\tau}^{0} \lambda^*(\eta)u(t+\eta)d\eta + r(t) \tag{2.15}$$

where

$$\theta_{\mathrm{x}}^* = \theta^* e^{a\eta}, \qquad \lambda^*(t) = \theta^* e^{a\eta}$$

Therefore, a choice of a control input of the form

$$u(t) = \theta_x(t)x(t) + \int_{-\tau}^{0} \lambda(t,\eta)u(t+\eta)d\eta + r(t) \tag{2.16}$$

leads to a closed-loop system of the form

$$\begin{aligned}\dot{x}(t) &= ax(t) + \theta^* \left[e^{a\tau}x(t-\tau) + \int_{-\tau}^{0} e^{-a\eta}u(t-\tau+\eta)d\eta \right] \\ &+\tilde{\theta}_x(t-\tau)x(t-\tau) + \int_{-\tau}^{0} \tilde{\lambda}(t-\tau,\eta)u(t-\tau+\eta)d\eta + r(t-\tau)\end{aligned} \tag{2.17}$$

where

$$\tilde{\theta}_x(t) = \theta_x(t) - \theta_x^*, \qquad \tilde{\lambda}(t,\eta) = \lambda(t,\eta) - \lambda^*.$$

From (2.8), it follows that (2.17) can be written as

$$\begin{aligned}\dot{x}(t) &= a_m x(t) + \tilde{\theta}_x(t-\tau)x(t-\tau) + \int_{-\tau}^{0} \tilde{\lambda}(t-\tau,\eta)u(t-\tau+\eta)d\eta \\ &+ r(t-\tau)\end{aligned} \tag{2.18}$$

As a result, defining $e(t) = x(t) - x_m(t)$, (2.18) and (2.13) imply that the underlying error model is of the form

$$\dot{e}(t) = a_m e(t) + \tilde{\theta}_x(t-\tau)x(t-\tau) + \int_{-\tau}^{0} \tilde{\lambda}(t-\tau,\eta)u(t-\tau+\eta)d\eta. \tag{2.19}$$

This error model is discussed in Section 2.3, where a Lyapunov-Krasovskii functional leads to semi-global stability in τ. Here, we give the stability result and leave the proof to Section 2.3, where the general case, n^{th} order system, is investigated.

Theorem 1 Given initial conditions $\tilde{\theta}_x(0)$, $x(\xi)$, $\tilde{\lambda}(\xi,\eta)$ for $\xi \in [-\tau, 0]$ and $u(\zeta)$ for $\zeta \in [-2\tau, 0]$, there exists a τ^* such that for all $\tau \in [0, \tau^*]$, the plant in (2.1),

controller in (2.16), and adaptive laws given by

$$\begin{aligned} \dot{\theta}_{\mathrm{x}}(t) &= -\gamma_1 e(t)x(t-\tau) \\ \frac{\partial \lambda}{\partial t}(t,\eta) &= -\gamma_\lambda e(t)u(t+\eta-\tau) \end{aligned} \tag{2.20}$$

have bounded solutions for all $t \geqslant 0$.

2.2 State variables accessible

The plant considered here is of the form

$$\dot{x}(t) = Ax(t) + bku(t-\tau) \tag{2.21}$$

where A and k are an unknown matrix and a scalar, respectively, (A, b) is controllable, and b is a known vector. We choose a reference model of the form

$$\dot{x}_{\mathrm{m}}(t) = A_{\mathrm{m}}x(t) + br(t-\tau) \tag{2.22}$$

where A_{m} is a suitable Hurwitz matrix. Taking a cue from Eq. (2.16) in the previous section, we choose a control input of the form

$$u(t) = \theta_{\mathrm{x}}^T(t)x(t) + \int_{-\tau}^{0} \lambda(t,\eta)u(t+\eta)d\eta + \theta_{\mathrm{r}}(t)r(t) \tag{2.23}$$

and adaptive laws of the form

$$\begin{aligned} \dot{\theta}_{\mathrm{x}}(t) &= -\gamma_1 e^T Pbx(t-\tau) \\ \dot{\lambda}(t,\eta) &= -\gamma_\lambda e^T Pbu(t-\tau+\eta) \\ \dot{\theta}_{\mathrm{r}}(t) &= -\gamma_{\mathrm{r}} e^T(t)Pbr(t-\tau) \end{aligned} \tag{2.24}$$

We show below that the closed-loop system specified by (2.21)-(2.24) leads to semi-global boundedness in τ. The desired parameters for $\theta_{\mathrm{x}}(t)$, $\lambda(t,\eta)$ and $\theta_{\mathrm{r}}(t)$ are defined

as

$$\begin{aligned} \theta_{\mathrm{x}}^{*} &= e^{A^{T}\tau}\theta^{*} \\ \lambda^{*}(\eta) &= \theta^{*T}e^{A\tau}bk \qquad (2.25) \\ \theta_{\mathrm{r}}^{*}k &= 1 \qquad (2.26) \end{aligned}$$

where

$$A + bk\theta^{*T} = A_{\mathrm{m}}. \qquad (2.27)$$

This in turn, after several algebraic manipulations, leads to an error equation of the form

$$\begin{aligned} \dot{e}(t) &= A_{\mathrm{m}}e(t) + bk[\tilde{\theta}_{\mathrm{x}}(t-\tau)x(t-\tau) + \int_{-\tau}^{0}\tilde{\lambda}(t-\tau,\eta)u(t-\tau+\eta)d\eta \\ &\quad +\tilde{\theta}_{\mathrm{r}}(t-\tau)r(t-\tau)] \qquad (2.28) \end{aligned}$$

As in Section 2.1, using a Lyapunov Krasovskii functional, (2.24) and (2.28) can be shown to have semi-globally bounded solutions. The underlying Theorem is stated below:

Theorem 2 Given initial conditions $\tilde{\theta}_{\mathrm{x}}(0)$, $\tilde{\theta}_{\mathrm{r}}(0)$, $x(\xi)$, $\tilde{\lambda}(\xi,\eta)$ for $\xi \in [-\tau, 0]$ and $u(\zeta)$ for $\zeta \in [-2\tau, 0]$, there exists a τ^{*} such that for all $\tau \in [0, \tau^{*}]$, the plant in (2.21), controller in (2.23), and adaptive laws given in (2.24) have bounded solutions for all $t \geqslant 0$.

2.3 Adaptive Posicast Control in the presence of input-output measurements with $n^{*} \leqslant 2$

In this section, the focus is on higher order time delay systems with relative degree, n^{*}, less than or equal to two.

2.3.1 Exact model matching for delayed systems

Consider the plant with the time delay τ whose input-output description is given as

$$y(t) = W_{\mathrm{p}}(s)u(t-\tau), \qquad W_{\mathrm{p}}(s) = k_{\mathrm{p}}\frac{Z_{\mathrm{p}}(s)}{R_{\mathrm{p(s)}}} \tag{2.29}$$

where $Z_{\mathrm{p}}(s)$ and $R_{\mathrm{p}}(s)$ are monic coprime polynomials with order m and n and $n^* = n - m > 0$ is defined as the relative order of the finite dimensional part of the plant. It is also assumed that $Z_{\mathrm{p}}(s)$ is Hurwitz and k_{p} is a constant gain parameter. The reference input-output description is given by

$$y_{\mathrm{m}}(t) = W_{\mathrm{m}}(s)r(t-\tau), \qquad W_{\mathrm{m}}(s) = k_{\mathrm{m}}\frac{Z_{\mathrm{m}}(s)}{R_{\mathrm{m}}(s)} \tag{2.30}$$

where $Z_{\mathrm{m}}(s)$ and $R_{\mathrm{m}}(s)$ are monic Hurwitz polynomials of degrees m_{m} and n_{m} respectively, and k_{m} is a constant gain parameter. Further, it is assumed that $n_{\mathrm{m}} - m_{\mathrm{m}} \geqslant n - m$.

The model matching problem is to determine a bounded control input $u(t)$ to the plant such that the closed loop transfer transfer function of the plant together with the controller, from $r(t)$ to $y_{\mathrm{p}}(t)$, matches the reference model transfer function.

Consider the following state space representation of the plant dynamics (2.29), together with two "signal generators" formed by a controllable pair Λ, l:

$$\dot{x}_{\mathrm{p}}(t) = A_{\mathrm{p}}x_{\mathrm{p}}(t) + b_{\mathrm{p}}u(t-\tau), \;\; y(t) = h_{\mathrm{p}}^T x_{\mathrm{p}}(t) \tag{2.31}$$

$$\dot{\omega}_1(t) = \Lambda\omega_1(t) + lu(t-\tau) \tag{2.32}$$

$$\dot{\omega}_2(t) = \Lambda\omega_2(t) + ly(t) \tag{2.33}$$

where, $\Lambda \in \Re^{nxn}$ and $l \in \Re^n$. Defining $\bar{x}(t) \triangleq x(t+\tau)$, $\bar{\omega}_i(t) \triangleq \omega_i(t+\tau)$, $i = 1, 2$, $\bar{y}(t) \triangleq y(t+\tau)$, (2.31)-(2.33) can be rewritten in the following form:

$$\dot{\bar{x}}_{\mathrm{p}}(t) = A_{\mathrm{p}}\bar{x}_{\mathrm{p}}(t) + b_{\mathrm{p}}u(t), \;\; \bar{y}(t) = h_{\mathrm{p}}^T\bar{x}_{\mathrm{p}}(t) \tag{2.34}$$

$$\dot{\bar{\omega}}_1(t) = \Lambda\bar{\omega}_1(t) + lu(t) \tag{2.35}$$

$$\dot{\bar{\omega}}_2(t) = \Lambda\bar{\omega}_2(t) + l\bar{y}(t) \tag{2.36}$$

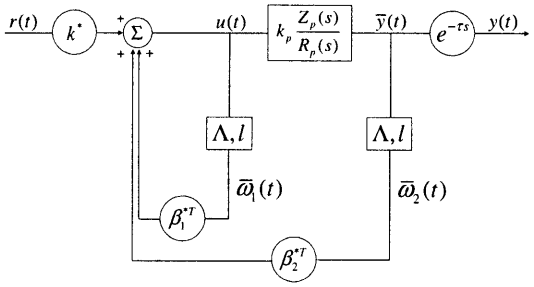

Figure 2-1: Exact model matching, Controller NC.

Under our assumptions, it follows [18] that there exists $\beta_1^*, \beta_2^* \in R^n$ and $k^* \in R$ sush that the control law

$$u(t) = \beta_1^{*T}\bar{\omega}_1(t) + \beta_2^{*T}\bar{\omega}_2(t) + k^* r(t) \tag{2.37}$$

satisfies the exact model matching condition.

$$\frac{\bar{y}(t)}{r(t)} = k_{\mathrm{m}} \frac{Z_{\mathrm{m}}(s)}{R_{\mathrm{m}}(s)}. \tag{2.38}$$

Note that the model matching is achieved between the rational parts of the closed loop transfer function and of the reference model. On the other hand, it follows directly from (2.38) that

$$\frac{y(t)}{r(t)} = k_{\mathrm{m}} \frac{Z_{\mathrm{m}}(s)}{R_{\mathrm{m}}(s)} e^{-\tau s} \tag{2.39}$$

which shows that the exact model matching condition is also satisfied between the total closed loop and the reference model transfer functions. Since $\bar{\omega}_2(t)$ requires the output measurement at time $t + \tau$, the control law given in (2.37) is non-causal. We refer to this closed loop system with the non-causal controller as "Controller NC" and it is depicted in Fig. 2-1.

It is also well known [18] that with zero initial conditions, there exists $c, d \in R^n$ such that $\bar{y}(t) = c^T\bar{\omega}_1(t) + d^T\bar{\omega}_2(t)$, which implies

$$y(t) = c^T\omega_1(t) + d^T\omega_2(t). \tag{2.40}$$

Substituting (2.40) into (2.33) and rewriting (2.32) and (2.33) together in vector-matrix form, we get

$$\begin{pmatrix} \dot{\omega}_1(t) \\ \dot{\omega}_2(t) \end{pmatrix} = A \begin{pmatrix} \omega_1(t) \\ \omega_2(t) \end{pmatrix} + bu(t-\tau)$$

$$\text{where, } A = \begin{bmatrix} \Lambda & 0 \\ lc^T & \Lambda + ld^T \end{bmatrix} \text{ and } b = \begin{bmatrix} l \\ 0 \end{bmatrix}. \tag{2.41}$$

From (2.41) we get

$$\begin{pmatrix} \bar{\omega}_1(t) \\ \bar{\omega}_2(t) \end{pmatrix} = e^{A\tau} \begin{pmatrix} \omega_1(t) \\ \omega_2(t) \end{pmatrix} + \int_{-\tau}^{0} e^{-A\sigma} bu(t+\sigma)\, \mathrm{d}\sigma. \tag{2.42}$$

Substituting (2.42) into (2.37) we obtain that

$$\begin{aligned} u(t) &= \left\{ \begin{bmatrix} \beta_1^{*T} & \beta_2^{*T} \end{bmatrix} e^{A\tau} \right\} \begin{pmatrix} \omega_1(t) \\ \omega_2(t) \end{pmatrix} \\ &\quad + \int_{-\tau}^{0} \left\{ \begin{bmatrix} \beta_1^{*T} & \beta_2^{*T} \end{bmatrix} e^{-A\sigma} b \right\} u(t+\sigma)\, \mathrm{d}\sigma \\ &\quad + k^* r(t), \end{aligned} \tag{2.43}$$

which can equivalently be expressed as

$$\begin{aligned} u(t) &= \alpha_1^{*T} \omega_1(t) + \alpha_2^{*T} \omega_2(t) + \int_{-\tau}^{0} \phi^*(\sigma) u(t+\sigma) \mathrm{d}\sigma \\ &\quad + k^* r(t). \end{aligned} \tag{2.44}$$

The controller (2.44) is causal and we refer to it as "Controller C". Defining $\beta^* = [\beta_1^{*T} \ \beta_2^{*T}]$ and $\alpha^* = [\alpha_1^{*T} \ \alpha_2^{*T}]$, we get the following relationships between the controller parameters of Controller NC and Controller C

$$\alpha^* = \beta^* e^{A\tau} \tag{2.45}$$

$$\phi^*(\sigma) = \beta^* e^{-A\sigma} b. \tag{2.46}$$

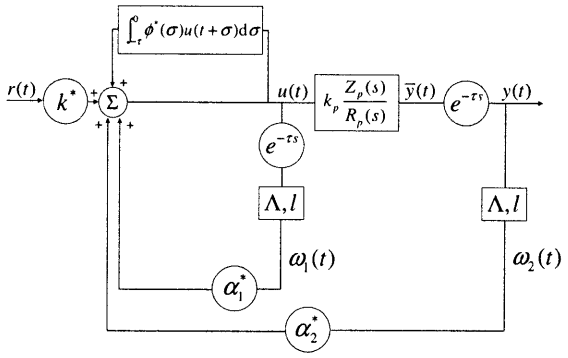

Figure 2-2: Exact model matching, Controller C.

The block diagram of Controller C is shown in Fig. 2-2.

In summary, an exact model matching controller, Controller C, can be designed for the time delay system (2.29) using a well known procedure for the delay free systems [18]. Note that the equivalence between Controller NC and Controller C shows that the latter relies on predicting the future output, $\bar{y}(t)$ to achieve exact model matching. This can be viewed as an equivalence result for higher order systems similar to that shown in Section 2.1 between (2.11) and (2.15).

Note that the model matching controller (2.44) was already introduced in [16] and [12]. The main contribution here is that we derive this controller by using the delay free part of the system dynamics, which considerably simplifies the design. In addition, instead of proposing a controller structure and proving that it is a model matching controller, we *derive* the controller using future state prediction which gives an insight about the controller structure. Finally, this derivation removes the assumption that the plant has poles with multiplicity one, which was assumed in the earlier papers. A similar result is given in [69] where it is stated that state prediction is a fundamental concept for time delay systems.

2.3.2 Adaptive Controller

The goal of this section is to design a model reference adaptive controller, motivated by the equivalence of the Controller NC and Controller C, for the plant described in (2.29) with unknown coefficients for the polynomials $Z_{\mathrm{p}}(s)$ and $R_{\mathrm{p}}(s)$ and with unknown, positive high frequency gain k_{p}. To start with, we assume that the relative

degree of the plant is one. The first step of the adaptive controller design is to design a fixed controller which satisfies the exact model matching with the reference model assuming that the plant parameters are known. This step was already completed in Section 2.3.1 resulting in the controller given in (2.44). In the second step, the controller parameters $\alpha_1^*, \alpha_2^*, \phi^*(\sigma)$ and k^* are replaced by time-varying parameters $\alpha_1(t), \alpha_2(t), \phi(t,\sigma)$ and $k(t)$ and the goal is to determine the laws by which they are adjusted so as to result in a stable system.

We define the following parameters:

$$
\begin{aligned}
&\tilde{k}(t) \triangleq k(t) - k^*, && \tilde{\alpha}_1(t) \triangleq \alpha_1(t) - \alpha_1^*,\\
&\tilde{\alpha}_2(t) \triangleq \alpha_2(t) - \alpha_2^*, && \tilde{\phi}(t,\sigma) \triangleq \phi(t,\sigma) - \phi^*,\\
&\alpha(t) \triangleq \left[\alpha_1^T(t)\ \alpha_2^T(t)\right]^T, && \beta(t) \triangleq \left[\beta_1^T(t)\ \beta_2^T(t)\right]^T,\\
&\Omega(t) \triangleq \left[\omega_1^T(t)\ \omega_2^T(t)\ r(t)\right]^T, && \omega(t) \triangleq \left[\omega_1^T(t)\ \omega_2^T(t)\right]^T,\\
&\theta(t) \triangleq \left[\alpha_1^T(t)\ \alpha_2^T(t)\ k(t)\right]^T, && \tilde{\theta}(t) \triangleq \theta(t) - \theta^*,\\
&\theta^* \triangleq \left[(\alpha_1^*)^T\ (\alpha_2^*)^T\ k^*\right]
\end{aligned}
$$

Consider a controller

$$
\begin{aligned}
u(t) &= \alpha^T(t)\omega(t) + \int_{-\tau}^{0} \phi(t,\sigma)u(t+\sigma)\mathrm{d}\sigma + k(t)r(t)\\
&= \alpha_1^{*T}\omega_1(t) + \alpha_2^{*T}\omega_2(t) + \int_{-\tau}^{0} \phi^*(\sigma)u(t+\sigma)\mathrm{d}\sigma\\
&\quad + k^*r(t) + \tilde{\alpha}_1^T(t)\omega_1(t) + \tilde{\alpha}_2^T(t)\omega_2(t)\\
&\quad + \int_{-\tau}^{0} \tilde{\phi}(t,\sigma)u(t+\sigma)\mathrm{d}\sigma + \tilde{k}(t)r(t). \qquad (2.47)
\end{aligned}
$$

Using the equivalence between (2.37) and (2.44), we can rewrite (2.47) as

$$
\begin{aligned}
u(t) &= \beta_1^{*T}\bar{\omega}_1(t) + \beta_2^{*T}\bar{\omega}_2(t) + k^*r(t) + \tilde{\alpha}_1^T(t)\omega_1(t)\\
&\quad + \tilde{\alpha}_2^T(t)\omega_2(t) + \int_{-\tau}^{0} \tilde{\phi}(t,\sigma)u(t+\sigma)\mathrm{d}\sigma\\
&\quad + \tilde{k}(t)r(t). \qquad (2.48)
\end{aligned}
$$

The differential equations, describing the plant (2.31) together with the controller

(2.48) can then be represented as

$$\begin{aligned}\dot{X}_{\rm p}(t) &= A_{\rm m}X_{\rm p}(t) + b_{\rm m}[\tilde{\theta}^T(t-\tau)\Omega(t-\tau) \\ &\quad + \int_{-\tau}^{0}\tilde{\phi}(t-\tau,\sigma)u(t-\tau+\sigma)\mathrm{d}\sigma + k^*r(t-\tau)], \\ y_{\rm p}(t) &= h_{\rm m}^T X_{\rm p}(t)\end{aligned} \tag{2.49}$$

where

$$\begin{aligned}A_{\rm m} &\triangleq \begin{bmatrix} A_{\rm p} & b_{\rm p}\beta_1^{*T} & b_{\rm p}\beta_2^{*T} \\ 0 & \Lambda + l\beta_1^{*T} & l\beta_2^{*T} \\ lh_{\rm p}^T & 0 & \Lambda \end{bmatrix}, \; b_{\rm m} \triangleq \begin{bmatrix} b_{\rm p} \\ l \\ 0 \end{bmatrix}, \\ X_{\rm p}(t) &\triangleq \left[x_{\rm p}^T(t) \;\; \omega_1^T(t) \;\; \omega_2^T(t)\right]^T, \; h_{\rm m}^T \triangleq \left[h_{\rm p}^T \;\; 0 \;\; 0\right], \\ y_{\rm p} &= y.\end{aligned} \tag{2.50}$$

We showed in Section 2.3.1 that when the parameter errors are equal to zero, the closed loop transfer function is identical to that of the reference model. Therefore, the reference model can be described by the $(3n)th$ order differential equation

$$\dot{X}_{\rm m}(t) = A_{\rm m}X_{\rm m}(t) + b_{\rm m}k^*r(t-\tau), \; y_{\rm m}(t) = h_{\rm m}^T X_{\rm m}(t) \tag{2.51}$$

where,

$$\begin{aligned}X_{\rm m}(t) &\triangleq \left[x_{\rm p}^{*T} \;\; \omega_1^{*T} \;\; \omega_2^{*T}\right]^T, \\ h_{\rm m}^T\left(sI - A_{\rm m}\right)^{-1} b_{\rm m}k^* &= k_{\rm m}\frac{Z_{\rm m}}{R_{\rm m}}.\end{aligned} \tag{2.52}$$

Note that $x_{\rm p}^*(t), \omega_1^*(t)$ and $\omega_2^*(t)$ can be considered as the signals in the reference model corresponding to $x_{\rm p}(t), \omega_1(t)$ and $\omega_2(t)$ in the closed loop system. Therefore, subtracting (2.51) from (2.49), we get an error equation for the overall system as

$$\dot{e}(t) = A_{\rm m}e(t) + b_{\rm m}[\tilde{\theta}^T(t-\tau)\Omega(t-\tau)$$

$$+\int_{-\tau}^{0}\tilde{\phi}(t-\tau,\sigma)u(t-\tau+\sigma)\mathrm{d}\sigma],$$

$$e_1(t)=h_{\mathrm{m}}^{T}e(t). \tag{2.53}$$

where $e(t)=X_{\mathrm{p}}-X_{\mathrm{m}}$ and $e_1(t)=y_{\mathrm{p}}(t)-y_{\mathrm{m}}(t)$.

The adaptive control law which guarantees convergence of the tracking error to zero and boundedness of all signals has the following form:

$$\begin{aligned}\dot{\tilde{\alpha}}(t) &= -\gamma_{\alpha}e_1(t)\omega(t-\tau)\\ \dot{\tilde{\phi}}(t,\sigma) &= -\gamma_{\phi}e_1(t)u(t-\tau+\sigma),-\tau\leqslant\sigma\leqslant 0\end{aligned} \tag{2.54}$$

where, γ_{α} and γ_{ϕ} are positive, real adaptation gains.

When the relative degree n^* equal to unity, it is easy to define a strictly positive real reference model $W_{\mathrm{m}}(s)$. When $n^*=2$, an addition of an input u_{a} to u as

$$\begin{aligned}u_{\mathrm{a}} &= \dot{\theta}^{T}\Omega^{'}+\int_{-\tau}^{0}\dot{\phi}(t,\sigma)u^{'}(t+\sigma)\mathrm{d}\sigma,\\ \dot{\Omega}^{'} &= -aI\Omega^{'}+\Omega,\\ \dot{u}^{'} &= -au^{'}+u,\quad a>0\end{aligned} \tag{2.55}$$

can be used to derive yet another error equation of the form

$$e(t)=W_{\mathrm{m}}(s)(s+a)e^{-s\tau}\left[\tilde{\theta}^{T}(t)\Omega(t)+\int_{-\tau}^{0}\tilde{\phi}(t,\sigma)u(t+\sigma)\mathrm{d}\sigma\right] \tag{2.56}$$

where $a>0$ is chosen such that $(s+a)W_{\mathrm{m}}(s)$ is strictly positive real. Therefore it suffices to consider the stability of (2.53). The results can then be extended to the case when $n^*=2$ by making use of the additional input u_{a}.

2.3.3 Stability Analysis

The following theorem confirms the desirable properties of the adaptive control law (2.54).

Theorem 2 Given initial conditions $x_p(0)$, $u(\eta)$, $\eta \in [t_0 - 2\tau, t_0]$, $\tilde{\alpha}(\xi), \tilde{\phi}(\xi)$, $\xi \in [t_0 - \tau, t_0]$, $\exists \tau^*$ s.t. $\forall \tau \in [0, \tau^*]$, the plant (2.29), the controller (2.47), and the adaptive laws given by (2.54) have bounded solutions $\forall t \geqslant 0$ and $lim_{t\to\infty} e_1(t) \to 0$.

We first state and prove the following lemma.

Lemma 1 Suppose a variable $u(t)$ is of the form

$$u(t) = f(t) + \int_{-\tau}^{0} \phi(t,\sigma)u(t+\sigma)\mathrm{d}\sigma \tag{2.57}$$

where $u, f : [t_0-\tau, \infty) \to \Re$, $\phi : [t_0, \infty)\mathrm{x}[-\tau, 0] \to \Re$ and constants $t_i^{'}$, $\bar{f}, c_0, c_1 \in \Re^+$ exist such that $\|f(t)\| \leqslant \bar{f}$,

$$\int_{-\tau}^{0} \phi^2(t,\sigma)\mathrm{d}\sigma \leqslant c_0^2, \tag{2.58}$$

and

$$\int_{-\tau}^{0} u^2(t+\sigma)d\sigma = c_1^2, \qquad \forall t \geqslant t_i^{'}. \tag{2.59}$$

Then,

$$\left|u(t_j^{'})\right| \leqslant 2(\bar{f} + c_1 c_0)e^{c_0^2(t_j^{'} - t_i^{'})}, \qquad \forall t_j^{'} \geqslant t_i^{'}. \tag{2.60}$$

Proof of Lemma 1 Since (2.57) is an implicit integral equation, we derive inequality (2.60) by considering a sequence u_n, and let u be the limit of this sequence as $n \to \infty$ [70].

Define

$$\begin{aligned} u_0(t_j^{'}) &\triangleq u(t_j^{'}), \qquad t_j^{'} < t_i^{'} \\ &\triangleq 0, \qquad\quad t_j^{'} \geqslant t_i^{'} \end{aligned} \tag{2.61}$$

$$
\begin{aligned}
u_{n+1}(t_j^{'}) &\triangleq u(t_j^{'}), \qquad t_j^{'} < t_i^{'}, \\
&\triangleq \int_{-\tau}^{0} \phi(t_j^{'}, \sigma) u_n(t_j^{'} + \sigma) \mathrm{d}\sigma + f(t_j^{'}), \qquad t_j^{'} \geqslant t_i^{'}, \\
&\quad n = 0, 1..\infty
\end{aligned} \tag{2.62}
$$

For $t_j^{'} \geqslant t_i^{'}$ and $n = 1$, we have that

$$
\begin{aligned}
\left| u_1(t_j^{'}) - u_0(t_j^{'}) \right| &= |f(t_j^{'}) + \int_{-\tau}^{0} \phi(t_j^{'}, \sigma) u_0(t_j^{'} + \sigma) \mathrm{d}\sigma| \\
&\leqslant \bar{f} + \left(\int_{-\tau}^{0} \left(\phi(t_j^{'}, \sigma) \right)^2 \mathrm{d}\sigma \right)^{1/2} \left(\int_{-\tau}^{0} \left(u(t_i^{'} + \sigma) \right)^2 \mathrm{d}\sigma \right)^{1/2}
\end{aligned} \tag{2.63}
$$

since the last parenthesis on the right hand side is being calculated over the time interval $[t_i^{'} - \tau, t_i^{'}]$. Using (2.58) and (2.59), (2.63) can be rewritten as

$$
\left| u_1(t_j^{'}) - u_0(t_j^{'}) \right| \leqslant \bar{f} + c_0 c_1 \tag{2.64}
$$

For $t_j^{'} \geqslant t_i^{'}$ and $n = 2$ we have that

$$
\begin{aligned}
\left| u_2(t_j^{'}) - u_1(t_j^{'}) \right| &= \left| \int_{-\tau}^{0} \phi(t_j^{'}, \sigma) \left(u_1(t_j^{'} + \sigma) - u_0(t_j^{'} + \sigma) \right) \mathrm{d}\sigma \right| \\
&\leqslant \left(\int_{-\tau}^{0} \phi^2(t_j^{'}, \sigma) \right)^{1/2} \left(\int_{-\tau}^{0} \left| u_1(t_j^{'} + \sigma) - u_0(t_j^{'} + \sigma) \right|^2 \mathrm{d}\sigma \right)^{1/2}
\end{aligned} \tag{2.65}
$$

Using inequality (2.58) and a change of variables $\zeta = t + \sigma$, (2.65) becomes

$$
\begin{aligned}
\left| u_2(t_j^{'}) - u_1(t_j^{'}) \right| &\leqslant c_0 \left(\int_{t_j^{'} - \tau}^{t_j^{'}} |u_1(\zeta) - u_0(\zeta)|^2 \mathrm{d}\zeta \right)^{1/2} \\
&= c_0 \left(\int_{t_j^{'} - \tau}^{t_i^{'}} |u_1(\zeta) - u_0(\zeta)|^2 \mathrm{d}\zeta + \int_{t_i^{'}}^{t_j^{'}} |u_1(\zeta) - u_0(\zeta)|^2 \mathrm{d}\zeta \right)^{1/2}
\end{aligned} \tag{2.66}
$$

We know from (2.61) and (2.62) that $u_1(\zeta) - u_0(\zeta) = 0$ for $\zeta < t_i^{'}$. Therefore, (2.66) can be further simplified as

$$\left|u_2(t_j^{'}) - u_1(t_j^{'})\right| \leqslant c_0 \left(\int_{t_i^{'}}^{t_j^{'}} |u_1(\zeta) - u_0(\zeta)|^2 \, \mathrm{d}\zeta \right)^{1/2} \tag{2.67}$$

Substituting (2.64) into (2.67) we obtain that

$$\left|u_2(t_j^{'}) - u_1(t_j{}^{'})\right| \leqslant \left(\bar{f} + c_1 c_0\right) c_0 \sqrt{(t_j^{'} - t_i^{'})} \tag{2.68}$$

Continuing this procedure iteratively, we obtain that

$$\left|u_{n+1}(t_j^{'}) - u_n(t_j^{'})\right| \leqslant \left(\bar{f} + c_1 c_0\right) \left(\frac{\left(c_0^2 (t_j^{'} - t_i^{'})\right)^n}{n!} \right)^{1/2}. \tag{2.69}$$

Note that the term $(t_j^{'} - t_i^{'})^n / n!$ in (2.69) is obtained due to successive integrations of $(t_j^{'} - t_i^{'})$. It can be shown using the ratio test [71] that the series $\sum_{n=1}^{\infty} \left(\bar{f} + c_0 c_1\right) \left(\frac{\left(c_0^2 (t - t_i^{'})\right)^n}{n!} \right)^{1/2}$ converges. This in turn implies that if S is defined as

$$S = \sum_{n=1}^{\infty} (u_n - u_{n-1}) \tag{2.70}$$

it can be shown that

$$S \leqslant 2(\bar{f} + c_1 c_0) e^{c_0^2 (t_j^{'} - t_i^{'})}. \tag{2.71}$$

Please see Appendix A for a proof of (2.71).

Defining $u \triangleq \lim_{n \to \infty} u_n$, from (2.70) and (2.71), we obtain that

$$\left|u(t_j^{'}) - u_0(t_j^{'})\right| \leqslant 2(\bar{f} + c_1 c_0) e^{c_0^2 (t_j^{'} - t_i^{'})} \tag{2.72}$$

This implies that,

$$\left|u(t_j^{'})\right| \leqslant 2(\bar{f} + c_1 c_0) e^{c_0^2 (t_j^{'} - t_i^{'})} \qquad t_j^{'} \geqslant t_i^{'} \tag{2.73}$$

and this completes the proof. Next, we describe the proof of Theorem 1.

Proof of Theorem 2 The proof is provided using the method of induction. Let

the statement S be given by

$$S : \|X_p(\xi)\| \leqslant I_0, \quad |u(\xi)| \leqslant U(I_0) \quad \forall \xi \in [t_0, t_0 + k\tau) \tag{2.74}$$

where $U(\cdot)$ is an analytic, bounded function of its arguments.

We note that $X_p(\xi)$ and $u(\xi)$ is bounded for $\xi \in [t_0 - 2\tau, t_0)$. Using this fact, we complete the proof by showing that

I. S is true for $k = 1$.

II. If S is true for k, then it is true for $k + 1$

I and II allow us to conclude that all signals are bounded for all $t \geqslant t_0$. Finally, from Barbalat's Lemma, convergence of the error e to zero follows.

I. S is true for $k = 1$.

The proof of I is given in three steps, each of which starts with a brief summary.

Step 1. *Some bounds on the signals are assumed in the time interval $[t_0 - 2\tau)$ and the negative semi-definiteness of the Lyapunov functional time derivative in $[t_0, t_0 + \tau)$ is shown, which yields the boundedness of the signals in $[t_0, t_0 + \tau)$. In addition, using Lemma 1, an upper bound for the control signal $u(t)$ in $[t_0, t_0 + \tau)$ is given.*

Consider a Lyapunov Functional

$$\begin{aligned} V(t) &= e(t)^T P e(t) + \tilde{\theta}(t)^T \tilde{\theta}(t) + \int_{-\tau}^{0} \tilde{\phi}(t, \sigma)^2 \mathrm{d}\sigma \\ &\quad + \int_{-\tau}^{0} \int_{t+\nu}^{t} \dot{\tilde{\theta}}(\xi)^T \dot{\tilde{\theta}}(\xi) \mathrm{d}\xi \mathrm{d}\nu \\ &\quad + \int_{-\tau}^{0} \int_{t+\nu}^{t} \int_{-\tau}^{0} \left(\dot{\tilde{\phi}}(\xi, \sigma) \right)^2 \mathrm{d}\sigma \mathrm{d}\xi \mathrm{d}\nu \end{aligned} \tag{2.75}$$

where $P > 0$. The error model (2.53) and the Lyapunov Functional (2.75) has been discussed in [19]. After algebraic manipulations, upper bound on the Lypaunov Function derivative can be computed as follows:

$$\dot{V}(t) \leqslant -e(t)^T [Q - 2\tau (\|\omega(t - \tau)\|^2$$

$$+\int_{-\tau}^{0}\|u(t-\tau+\sigma)\|^2\,\mathrm{d}\sigma)h_{\mathrm{m}}h_{\mathrm{m}}^T]e(t) \tag{2.76}$$

where $Q>0$ satisfies $A_{\mathrm{m}}^TP+PA_{\mathrm{m}}=-Q$. For the non-postiveness of $\dot{V}(t)$, we need to satisfy

$$Q-2\tau\left(\|\omega(t-\tau)\|^2+\int_{-\tau}^{0}\|u(t-\tau+\sigma)\|^2\,\mathrm{d}\sigma\right)h_{\mathrm{m}}h_{\mathrm{m}}^T\geqslant 0 \tag{2.77}$$

Since ω and u are dependent variables, condition (2.77) may not be easy to check. Note however that the bound on $\dot{V}(t)$ is given by some bounds on ω defined at $t-\tau$ and on u defined on the whole interval $[t-2\tau,t-\tau]$. It is shown below that this condition can be replaced by bounds on signals ω and u over the time interval $[t_0-\tau,t_0]$ and $[t_0-2\tau,t_0]$, respectively.

Suppose that

$$\sup_{\xi\in[t_0-\tau,t_0)}\|\omega(\xi)\|^2 \leqslant \gamma_1 \tag{2.78}$$

$$\sup_{\xi\in[t_0-2\tau,t_0)}\|u(\xi)\|^2 \leqslant \gamma_2 \tag{2.79}$$

for some $\gamma_1>0$, $\gamma_2>0$ and a $\tau_1>0$ is such that

$$2\tau_1\left(\gamma_1+\gamma_2\right)h_{\mathrm{m}}h_{\mathrm{m}}^T<Q \tag{2.80}$$

Then, the following inequality is satisfied:

$$\begin{aligned}&Q-2\tau\left(\|\omega(\xi-\tau)\|^2+\int_{-\tau}^{0}\|u(\xi-\tau+\sigma)\|^2\,\mathrm{d}\sigma\right)h_{\mathrm{m}}h_{\mathrm{m}}^T>0,\\&\forall\xi\in[t_0,t_0+\tau),\forall\tau\in[0,\tau_1].\end{aligned} \tag{2.81}$$

It follows that $V(t)$ is non-increasing for $t\in[t_0,t_0+\tau)$. Thus, we have

$$\|X_{\mathrm{p}}(\xi)\|\leqslant\sqrt{\frac{V(t_0)}{\lambda_{min}(P)}}+\|X_{\mathrm{m}}(\xi)\| \tag{2.82}$$

and hence,

$$\|\omega(\xi)\| \leqslant \sqrt{\frac{V(t_0)}{\lambda_{min}(P)}} + \|X_{\mathrm{m}}(\xi)\|, \forall \xi \in [t_0, t_0 + \tau). \tag{2.83}$$

The inequality in (2.83) is due to the fact that ω is a part of the state vector X_{p}. We also have the following inequalities as a result of non-increasing Lyapunov functional:

$$\left\|\tilde{\theta}(\xi)\right\|^2 \leqslant V(t_0), \tag{2.84}$$

$$\left\|\int_{-\tau}^{0} \tilde{\phi}(\xi, \sigma)^2 \mathrm{d}\sigma\right\| \leqslant V(t_0). \tag{2.85}$$

To simplify the notation, we define

$$I_0 \triangleq \max\left(\sqrt{\frac{V(t_0)}{\lambda_{min}(P)}} + \|X_{\mathrm{m}}\|, V(t_0), \sqrt{V(t_0)}\right). \tag{2.86}$$

An upper bound on the control signal $u(t)$ for $t \in [t_0, t_0 + \tau)$ can be derived by using Lemma 1. In particular, setting $t_i' = t_0$, $t_j' = t_0 + \tau$, $c_0^2 = V(t_0)$ and using (2.47), (2.79), (2.84), (2.85) and (2.86), we obtain that

$$\begin{aligned} |u(\xi)| \;&\leqslant\; 2\left(\bar{f} + \left(\int_{-\tau}^{0} \left(u(t_0 + \sigma)\right)^2 \mathrm{d}\sigma\right)^{1/2} I_0\right) e^{I_0 \tau} \\ &\forall \quad \xi \in [t_0, t_0 + \tau), \end{aligned} \tag{2.87}$$

where $\bar{f}$ depends only on I_0. For simplicity, we will define $g(\gamma_2, I_0, \tau) \triangleq 2\left(\bar{f} + \gamma_2 I_0 \sqrt{\tau}\right) e^{I_0 \tau}$ and rewrite (2.87) as

$$|u(\xi)| \leqslant g(\gamma_2, I_0, \tau), \forall \xi \in [t_0, t_0 + \tau), \tag{2.88}$$

Step 2. *A delay value is found that leads to a non-increasing $\dot{V}$ over $[t_0, t_0 + 2\tau]$, which in turn shows that X_{p} is bounded over the same interval.*

Consider a delay value of $\tau_2 > 0$ that satisfies

$$2\tau_2 \left(I_0^2 + \left(\max(\gamma_2, g(\gamma_2, I_0, \tau_2))\right)^2 \tau_2\right) h_{\mathrm{m}} h_{\mathrm{m}}^T < Q. \tag{2.89}$$

For $\bar{\tau}_2 = \min(\tau_1, \tau_2)$, (2.77) is satisfied in the interval $[t_0, t_0 + 2\tau)$, for all $\tau \in [0, \bar{\tau}_2]$. Therefore, we obtain that

$$\|X_{\mathrm{p}}(\xi)\| \leqslant I_0, \forall \xi \in [t_0, t_0 + 2\tau)\,. \tag{2.90}$$

Step 3. *It is shown that the bound on the control signal u over the time interval* $[t_0, t_0 + \tau)$ *depends only on* $A_{\mathrm{p}}, b_{\mathrm{p}}, T, I_0$ *and* τ. *The proof given in this section is similar to the one given in [72], Lemma 5.*

Let $\Psi_{\mathrm{u}} = \{t|\ |u(t)| = \sup_{\sigma \leqslant t} |u(\sigma)|\}$.

Let $[t_i - \tau, t_i - \tau + T] \subset \Psi_{\mathrm{u}} \subset [t_0, t_0 + \tau)$. Defining $z(t) = u(t - \tau)$, we can solve (2.31) as

$$x_{\mathrm{p}}(t_i + T) = x_{\mathrm{p}}(t_i) e^{A_{\mathrm{p}} T} + \int_{t_i}^{t_i + T} e^{A_{\mathrm{p}}(T + t_i - t)} b_{\mathrm{p}} z(t) \mathrm{d}t \tag{2.91}$$

Positive constants c_6 and c_7 exists such that $||e^{A_{\mathrm{p}} T}|| \leqslant c_6$ and $||\int_0^T e^{A_{\mathrm{p}}\sigma} b_{\mathrm{p}} \mathrm{d}\sigma|| \geqslant c_7$ and

$$\|x_{\mathrm{p}}(t_i + T)\| \geqslant |c_7 |z(t_i)| - c_6 \|x_{\mathrm{p}}(t_i)\|| \tag{2.92}$$

Note that we obtain (2.92) by selecting T such that the terms of the vector $e^{A_{\mathrm{p}}\sigma} b_{\mathrm{p}}$ does not change sign for $\sigma \in [0, T]$. In addition, note that once T is selected properly, the inequality (2.92) is satisfied for any time interval $[t_j, t_j + T]$ as soon as $[t_j - \tau, t_j + T - \tau] \subset \Psi_{\mathrm{u}} \subset [t_0, t_0 + \tau)$ since the constants c_6 and c_7 are determined only by the size of T.

From (2.92) we obtain that

$$\|x_{\mathrm{p}}(t_i + T)\| + \|x_{\mathrm{p}}(t_i)\|\, c_6 \geqslant c_7\, |z(t_i)| \tag{2.93}$$

or

$$|u(t_i - \tau)| \leqslant \frac{c_6}{c_7} \|x_{\mathrm{p}}(t_i)\| + \frac{1}{c_7} \|x_{\mathrm{p}}(t_i + T)\| \tag{2.94}$$

Since x_{p} is a part of the state vector X_{p}, $\|x_{\mathrm{p}}(t)\| \leqslant \|X_{\mathrm{p}}(t)\|$, for any t. In addition, we find using (2.90) that $\|x_{\mathrm{p}}(t)\| \leqslant I_0$ in the time interval $[t_0, t_0 + 2\tau)$. Therefore, (2.94) can be simplified as

$$|u(t_i - \tau)| \leqslant \frac{(1 + c_6)}{c_7} I_0 \tag{2.95}$$

Using Lemma 1 by setting $t_i' = t_i - \tau$, $t_j' = t_i - \tau + T$ and $c_0^2 = V(t_0)$, using (2.86) and noting that $\left(\int_{-\tau}^{0} (u(t_i - \tau + \sigma))^2 \, \mathrm{d}\sigma\right)^{1/2} = c_1$, we obtain that

$$|u(t_i + T - \tau)| \leqslant 2 \left(\bar{f} + I_0 \sqrt{\int_{-\tau}^{0} (u(t_i - \tau + \sigma))^2 \, \mathrm{d}\sigma} \right) e^{I_0 T}. \tag{2.96}$$

Since $|u(t)| = \sup_{\sigma \leqslant t} |u(\sigma)|$ over $t \in [t_i - \tau, t_i + T - \tau]$, (2.96) can be simplified as

$$|u(t_i + T - \tau)| \leqslant 2 \left(\bar{f} + u(t_i - \tau) I_0 \sqrt{\tau} \right) e^{I_0 T} \tag{2.97}$$

Using (2.95), (2.97) can be simplified as

$$|u(t_i + T - \tau)| \leqslant 2 \left(\bar{f} + \frac{\sqrt{\tau}(1 + c_6)}{c_7} I_0^2 \right) e^{c_0 T} \tag{2.98}$$

Since $|u(t)| = \sup_{\sigma \leqslant t} |u(\sigma)|$ over $t \in [t_i - \tau, t_i - \tau + T]$ and t_i is any arbitrary time instant in $\Phi_{\mathrm{u}} \cap [t_0, t_0 + \tau)$, it follows that $\forall t \in \Psi_{\mathrm{u}} \cap [t_0, t_0 + \tau)$,

$$|u(t)| \leqslant 2 \left(\bar{f} + \frac{\sqrt{\tau}(1 + c_6)}{c_7} I_0^2 \right) e^{I_0 T}. \tag{2.99}$$

When $t \notin \Psi_{\mathrm{u}}$, the inequality (2.99) is strengthened further. Hence, it follows that the inequality holds for the whole interval $[t_0, t_0 + \tau)$. Note that the right hand side of the inequality is a function of $A_{\mathrm{p}}, b_{\mathrm{p}}, T$ and I_0. For simplicity, we are going to drop the dependence on $A_{\mathrm{p}}, b_{\mathrm{p}}$ and T and represents the inequality as in the following, which simplifies the notation:

$$|u(t)| \leqslant U(I_0),\ t \in [t_0, t_0 + \tau) \tag{2.100}$$

where U is a continuous function.

Step 4. *Finally, a uniform upper bound τ^* is given for the time delay τ such that I is satisfied.*

Let the delay value τ_3 satisfy the following inequality:

$$2\tau_3[I_0^2 + (\max(U(I_0), g(U(I_0), I_0, \tau_3)))^2 \tau_3]h_{\mathrm{m}}h_{\mathrm{m}}^T < Q. \tag{2.101}$$

For $\tau^* = \min(\bar{\tau}_2, \tau_3)$, the following inequalities hold:

$$\|X_{\mathrm{p}}(\xi)\| \leqslant I_0,\ \ |u(\xi)| \leqslant U(I_0)\ \ \forall \xi \in [t_0, t_0 + \tau)\ \ \forall \tau \in [0, \tau^*] \tag{2.102}$$

This completes the proof of I.

Note that, in Steps 1-3, I is proved for a delay value $\tau \in [0, \bar{\tau}_2]$. Finally in Step 4, a new upper bound, τ^*, is given for the allowable time delay τ. The need for the introduction of this new upper bound will be clear in the next section, where we prove II.

II. If S is true for k, then it is true for $k+1$

Assume that

$$\|X_{\mathrm{p}}(\xi)\| \leqslant I_0, \quad |u(\xi)| \leqslant U(I_0) \quad \xi \in [t_0, t_0 + k\tau]. \tag{2.103}$$

Then, using (2.101) we conclude that the Lyapunov function is non-increasing in the time interval $[t_0 + k\tau, t_0 + (k+1)\tau]$ since $\tau \leqslant \tau^* \leqslant \tau_3$. This means that $\|X_{\mathrm{p}}(t)\| \leqslant I_0$, and, using Lemma 1, $|u(t)| \leqslant g(U(I_0), I_0, \tau)$ for $t \in [t_0 + k\tau, t_0 + (k+1)\tau]$. Again, using (2.101) and the fact that $\tau \leqslant \tau^* \leqslant \tau_3$, we conclude that the Lyapunov function is non-increasing in the time interval $[t_0 + (k+1)\tau, t_0 + (k+2)\tau]$. Hence, $\|X_{\mathrm{p}}(t)\| \leqslant I_0$ for $t \in [t_0 + (k+1)\tau, t_0 + (k+2)\tau]$. But this means that $|u(t)| \leqslant U(I_0)$ for $t \in [t_0 + k\tau, t_0 + (k+1)\tau]$ using the same procedure as in Step 3. Therefore, we have that

$$\|X_{\mathrm{p}}(\xi)\| \leqslant I_0, \quad |u(\xi)| \leqslant U(I_0) \quad \xi \in [t_0, t_0 + (k+1)\tau] \tag{2.104}$$

This completes the proof of II.

Therefore, we proved the boundedness of the signals in the system, using induction. The second derivative of the Lyapunov functional includes these signals as well as their derivatives which can be shown to be bounded using the adaptation laws (2.54). Hence, the requirements of the Barbalat's Lemma are satisfied, which completes the stability proof. The extension to relative degree 2 case is similar to [19] and can be found therein.

2.3.4 Possible Nonlinear Extention

The method of using the future values of the system states in the fixed model matching controller and then developing an adaptive controller in the presence of uncertainties can also be used for simple nonlinear systems.

Consider the following nonlinear plant dynamics

$$\dot{x}_{\mathrm{p}}(t) = a x_{\mathrm{p}}^2(t) + u(t-\tau) \tag{2.105}$$

where a is a known constant. The goal is tracking the reference model, which is given as

$$\dot{x}_{\mathrm{m}}(t) = -x_{\mathrm{m}}(t). \tag{2.106}$$

This goal can be achieved by using the following control law

$$u(t) = -a x_{\mathrm{p}}^2(t+\tau) - x_{\mathrm{p}}(t+\tau) \tag{2.107}$$

The problem here is that the control law given in (2.107) is non-causal. However, defining $P(t) \triangleq x_{\mathrm{p}}(t+\tau)$, we can *predict* $x_{\mathrm{p}}(t+\tau)$ as [73]:

$$P(t) = \int_{t-\tau}^{t} b^*(\theta)P^2(\theta)\mathrm{d}\theta + c^* x_{\mathrm{p}}(t) + \int_{t-\tau}^{t} d^*(\theta)u(\theta)\mathrm{d}\theta \tag{2.108}$$

with an initial condition

$$P(\theta) = \int_{-\tau}^{\theta} b(\sigma)P^2(\sigma)\mathrm{d}\sigma + c x_{\mathrm{p}}(0) + \int_{-\tau}^{\theta} d(\sigma)u(\sigma)\mathrm{d}\sigma \tag{2.109}$$

for $\theta \in [-\tau, 0]$. Here, b, c and d are to be determined using the techniques given in [73].

When a is unknown, a control input of the form

$$\begin{aligned} u(t) \;=\; & \left(\int_{t-\tau}^{t} b(t,\theta)P(\theta)^2\mathrm{d}\theta\right)^2 + (c(t)x_{\mathrm{p}}(t))^2 \\ & + \left(\int_{t-\tau}^{t} d(t,\theta)u(\theta)\mathrm{d}\theta\right)^2 + c(t)x_{\mathrm{p}}(t)\int_{t-\tau}^{t} b(t,\theta)P^2(\theta)\mathrm{d}\theta \\ & + \int_{t-\tau}^{t} b(t,\theta)P^2(\theta)\mathrm{d}\theta \int_{t-\tau}^{t} d(t,\theta)u(\theta)\mathrm{d}\theta \\ & + c(t)x_{\mathrm{p}}(t)\int_{t-\tau}^{t} d(t,\theta)u(\theta)\mathrm{d}\theta \end{aligned} \tag{2.110}$$

where $\tilde{(\cdot)} = (\cdot)(t) - (\cdot)^*$, leads to a closed loop system of the form

$$\begin{aligned} \dot{x}_{\mathrm{p}}(t) \;=\; & -x_{\mathrm{p}}(t) + \left(\int_{t-2\tau}^{t-\tau} \tilde{b}(t-\tau,\theta)P^2(\theta)\mathrm{d}\theta\right)^2 + (\tilde{c}(t-\tau)x_{\mathrm{p}}(t-\tau))^2 \\ & + \left(\int_{t-2\tau}^{t-\tau} \tilde{d}(t-\tau,\theta)u(\theta)\mathrm{d}\theta\right)^2 \\ & + \tilde{c}(t-\tau)x_{\mathrm{p}}(t-\tau)\int_{t-2\tau}^{t-\tau} \tilde{b}(t-\tau,\theta)P^2(\theta)\mathrm{d}\theta \\ & + \int_{t-2\tau}^{t-\tau} \tilde{b}(t-\tau,\theta)P^2(\theta)\mathrm{d}\theta \int_{t-2\tau}^{t-\tau} \tilde{d}(t-\tau,\theta)u(\theta)\mathrm{d}\theta \\ & + \tilde{c}(t-\tau)x_{\mathrm{p}}(t-\tau)\int_{t-2\tau}^{t-\tau} \tilde{d}(t-\tau,\theta)u(\theta)\mathrm{d}\theta \end{aligned} \tag{2.111}$$

As a result, defining $e(t) = x_{\mathrm{p}}(t) - x_{\mathrm{m}}(t)$, (2.106) and (2.111) imply that the

underlying error model is of the form

$$\begin{aligned}
\dot{e}(t) &= -e(t) + \left(\int_{t-2\tau}^{t-\tau} \tilde{b}(t-\tau,\theta)P^2(\theta)\mathrm{d}\theta\right)^2 + (\tilde{c}(t-\tau)x_{\mathrm{p}}(t-\tau))^2 \\
&\quad + \left(\int_{t-2\tau}^{t-\tau} \tilde{d}(t-\tau,\theta)u(\theta)\mathrm{d}\theta\right)^2 \\
&\quad + \tilde{c}(t-\tau)x_{\mathrm{p}}(t-\tau)\int_{t-2\tau}^{t-\tau} \tilde{b}(t-\tau,\theta)P^2(\theta)\mathrm{d}\theta \\
&\quad + \int_{t-2\tau}^{t-\tau} \tilde{b}(t-\tau,\theta)P^2(\theta)\mathrm{d}\theta \int_{t-2\tau}^{t-\tau} \tilde{d}(t-\tau,\theta)u(\theta)\mathrm{d}\theta \\
&\quad + \tilde{c}(t-\tau)x_{\mathrm{p}}(t-\tau)\int_{t-2\tau}^{t-\tau} \tilde{d}(t-\tau,\theta)u(\theta)\mathrm{d}\theta
\end{aligned} \tag{2.112}$$

The stability of the closed loop system can be shown if a suitable Lyapunov function can be found for the error model (2.112).

2.4 Summary

In this chapter, we proposed the Adaptive Posicast Controller (APC) for time delay systems. The controller is based on the Smith Predictor and finite-spectrum assignment controller and modified so as to accommodate parametric uncertainties in the plant dynamics. We first proposed a model matching controller for time delay systems with known time delay, where, a non-causal controller is designed first, for the rational part of the plant dynamics. Then, by using the known delay value, the future prediction of the system states are calculated and used to show that the non-causal controller is equivalent to a causal controller. Using this equivalence, we derived the closed loop error dynamics for the APC and showed the stability of the overall system by defining a suitable Lyapunov-Krasovskii functional. A possible extension of this approach to nonlinear systems is also discussed.

Chapter 3

Spark Ignition Engine Idle Speed Control: An Adaptive Control Approach

3.1 Plant Model

The plant model for ISC explained in this chapter is standard [20]. The control input in the model is the throttle position in degrees and the output is the engine speed in revolutions-per-minute (rpm). Throttle-only control of engine speed is considered since our intent is to improve the performance of this loop without relying on the authority of the spark control. Below, the modeling aspects are discussed for each subsystem.

3.1.1 Throttle Mass Flow

The air mass flow thorough the throttle opening during idling can be modeled using the choked flow equation

$$\varpi_{\text{th}} = A_{\text{th}} \frac{p_{\text{a}}}{\sqrt{2RT_{\text{a}}}} \tag{3.1}$$

where, ϖ_{th} is the air mass flow rate passing thorough the throttle opening, A_{th} is the effective area of the throttle, p_{a} is the ambient pressure, T_{a} is the ambient temperature

and R is the gas constant. Note that the throttle area is a nonlinear function of the throttle position, but given that during idling the throttle movement is very small, a linear relationship between throttle position and throttle effective flow area can be assumed.

3.1.2 Intake Manifold

Assuming isothermal conditions, the intake manifold pressure dynamics can be modeled as

$$\frac{d}{dt}p_{\mathrm{m}} = \frac{RT_{\mathrm{m}}}{V_{\mathrm{m}}}(\varpi_{\mathrm{th}} - \varpi_{\mathrm{eng}}) \tag{3.2}$$

where, p_{m}, T_{m}, and V_{m} are the manifold pressure, temperature and volume respectively and ϖ_{eng} is the air mass flow rate exiting the intake manifold and entering the engine.

3.1.3 Engine Air Mass Flow

The mean value of the fuel-air mixture flow rate entering the engine cylinders can be approximated using the following equation:

$$\varpi_{\mathrm{mix}} = \eta_{\mathrm{v}}\frac{p_{\mathrm{m}}}{RT_{\mathrm{m}}}\frac{V_{\mathrm{d}}\omega_{\mathrm{e}}}{4\pi} \tag{3.3}$$

where, η_{v} is the volumetric efficiency, V_{d} is the displacement volume and ω_{e} is the engine speed in radians-per-second. Air mass flow rate entering the cylinders can be found using the formula $\varpi_{\mathrm{eng}} = \varpi_{\mathrm{mix}}/[1+\Phi(F/A)_{\mathrm{s}}]$, where $(F/A)_{\mathrm{s}}$ and Φ represent the stoichiometric fuel-to-air ratio and fuel-to-air ratio normalized by the stoichiometric fuel-to-air ratio, respectively. $\Phi = (F/A)/(F/A)_s$ is referred to as the equivalence ratio.

3.1.4 Torque Generation

In general, generated torque is a nonlinear function of engine speed, mass flow rate into the engine cylinders, equivalence ratio and spark advance:

$$T_e = f(N, \varpi_{mix}, \Phi, SA) \tag{3.4}$$

where SA represents the spark advance. This nonlinear relationship can be obtained with a least squares method using engine data. Also note that the induction to power (IP) delay enters into system dynamics through (3.4) as the torque depends on the delayed value of the mass flow rate into the engine cylinders.

3.1.5 Engine Rotational Dynamics

The equation of engine rotational dynamics is as follows:

$$\frac{d}{dt}\omega_e = \frac{1}{J}(T_e - T_l) \tag{3.5}$$

where, J is the engine inertia in neutral and T_l is the load torque on the engine including the internal engine friction.

3.1.6 Final Model for ISC

For ISC design, a nonlinear mean value engine model based on the above subsystem models is linearized around the nominal idle speed value (650 rpm) to obtain a linear plant model. Considering the deviation in the throttle position in degrees as the input and the deviation in engine speed in rpm as the output, the parametric transfer function of this linear model is

$$G(s) = K\frac{s^2 + n_1 s + n_2}{s^3 + d_1 s^2 + d_2 s + d_3}e^{-0.15s} \tag{3.6}$$

Note that the delay free part of the transfer function in (3.6) is third-order and relative degree one. The simplicity of (3.6) will subsequently be useful in determining

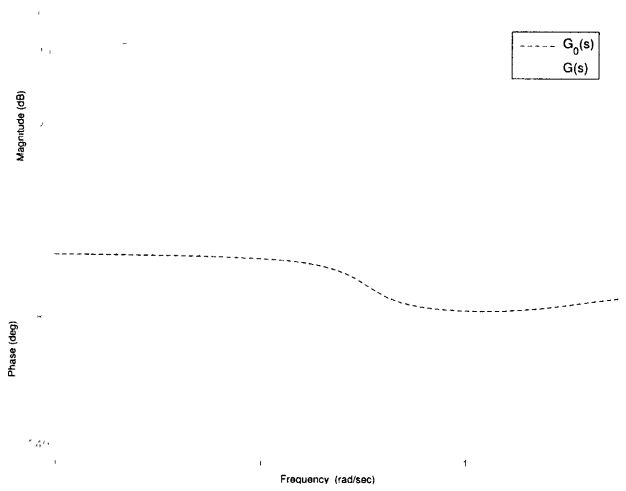

Figure 3-1: Bode plots of $G(s)$ and $G_0(s)$

the structure of the Adaptive Posicast Controller (APC).

The IP delay at the nominal idle speed of 650 rpm is 90 ms assuming that this delay is the result of 360 degrees of crank rotation or one revolution of the crank shaft. However, it is known that one revolution is only an approximation, since, for example, the maximum torque production does not occur exactly at the top dead center. In addition, the actuator delay and computational delays also contribute to the overall delay value. 150 ms time delay seen in (3.6) is a combined result of all these effects.

The parameter values for this nominal operating point were $K = 29.8$, $n_1 = 50$, $n_2 = 833$, $d_1 = 21.2$, $d_2 = 51.3$ and $d_3 = 189.5$. One should also note that these parameter values are valid only for the nominal operating point and thus are specific to certain values of engine speed, load torque, ambient pressure, ambient temperature and engine temperature. The input delay is used to approximate the effect of state delay in the model (3.1)-(3.5). Bode plots of the plant transfer function (3.6) with and without the delay, $G(s)$ and $G_0(s)$, are presented in Fig. 3-1, assuming the nominal parameter values. This figure clearly shows the rapid phase decrease with increasing frequency due to the time delay.

3.2 APC Design

3.2.1 Initial Design

APC is a model reference adaptive controller for systems with known input delay. Below, we summarize the main idea behind the APC. The reader is referred to [43] for additional details. Consider a linearized plant with input-output description given as

$$y(t) = W_{\mathrm{p}}(s)u(t-\tau), \qquad W_{\mathrm{p}}(s) = \frac{k_{\mathrm{p}}Z_{\mathrm{p}}(s)}{R_{\mathrm{p}}(s)} \tag{3.7}$$

where y is the measured plant output, u is the control input, and $W_{\mathrm{p}}(s)$ is the delay-free part of the plant transfer function. $R_{\mathrm{p}}(s)$ is the n^{th} order denominator polynomial, not necessarily stable and the numerator polynomial, $Z_{\mathrm{p}}(s)$ has only minimum phase zeros. The relative degree, n^*, which is equal to the order of the denominator minus the order of the numerator, is assumed to be smaller or equal to two. It is also assumed that the delay and the sign of the high frequency gain k_{p} are known, but otherwise $W_{\mathrm{p}}(s)$ may be unknown. Suppose that the reference model, reflecting desired response characteristics, is given as

$$y_{\mathrm{m}}(t) = W_{\mathrm{m}}(s)r(t-\tau), \qquad W_{\mathrm{m}}(s) = \frac{k_{\mathrm{m}}}{R_{\mathrm{m}}(s)} \tag{3.8}$$

where $R_{\mathrm{m}}(s)$ is a stable polynomial with degree n^*, k_{m} is the high frequency gain and r is the desired reference input.

Consider the following state space representation of the plant dynamics (3.7), together with two "signal generators" formed by a controllable pair Λ, l

$$\dot{x}_{\mathrm{p}}(t) = A_{\mathrm{p}}x_{\mathrm{p}}(t) + b_{\mathrm{p}}u(t-\tau), \;\; y(t) = h_{\mathrm{p}}^T x_{\mathrm{p}}(t) \tag{3.9}$$

$$\dot{\omega}_1(t) = \Lambda\omega_1(t) + lu(t-\tau) \tag{3.10}$$

$$\dot{\omega}_2(t) = \Lambda\omega_2(t) + ly(t) \tag{3.11}$$

where, $\Lambda \in \Re^{nxn}$ and $l \in \Re^n$. It follows [74] that there exist $k^* \in \Re$, α_1^{*T}, $\alpha_2^{*T} \in \Re^n$,

$\lambda^*(\sigma) : [-\tau, 0] \rightarrow \Re$ such that the control law

$$\begin{aligned} u(t) &= \alpha_1^{*T}\omega_1(t) + \alpha_2^{*T}\omega_2(t) + \int_{-\tau}^{0} \lambda^*(\sigma)u(t+\sigma)\mathrm{d}\sigma \\ &\quad + k^* r(t) \end{aligned} \tag{3.12}$$

satisfies the exact model matching condition.

$$\frac{y(t)}{r(t)} = \frac{k_\mathrm{m}}{R_\mathrm{m}(s)} e^{-\tau s}. \tag{3.13}$$

We now consider the control of the plant (3.7) when the transfer function $W_\mathrm{p}(s)$ has unknown coefficients and when the time delay τ is known. Consider the following adaptive controller [43]:

$$\begin{aligned} u(t) &= \alpha_1(t)^T\omega_1(t) + \alpha_2(t)^T\omega_2(t) + \int_{-\tau}^{0} \lambda(t,\sigma)u(t+\sigma)\mathrm{d}\sigma \\ &\quad + k(t)r(t), \\ \dot{\theta}(t) &= -\Gamma e_1(t)\Omega(t-\tau), \\ \frac{\partial\lambda(t,\sigma)}{\partial t} &= -\gamma_\lambda(\sigma)e_1(t)u(t+\sigma-\tau) \end{aligned} \tag{3.14}$$

where,

$$\theta = \begin{bmatrix} \alpha_1 \\ \alpha_2 \\ k \end{bmatrix}, \qquad \Omega = \begin{bmatrix} \omega_1 \\ \omega_2 \\ r \end{bmatrix}, \qquad e_1 = y - y_\mathrm{m}, \tag{3.15}$$

Γ is a diagonal matrix, the entries of which represent the adaptation rate of the corresponding controller parameter and $\gamma_\lambda(\sigma)$ is the adaptation rate for the controller parameter $\lambda(t,\sigma)$. Defining the parameter errors as $\tilde{\theta}(t) = \theta(t) - \theta^*$, $\tilde{\lambda}(t,\sigma) = \lambda(t,\sigma) - \lambda^*(\sigma)$, the control signal u in (3.14) can be rewritten as

$$\begin{aligned} u(t) &= \alpha^{*T}\omega(t) + \int_{-\tau}^{0} \lambda^*(\sigma)u(t+\sigma)\mathrm{d}\sigma \\ &\quad + k^* r(t) \\ &\quad + \tilde{\alpha}(t)^T\omega(t) + \int_{-\tau}^{0} \tilde{\lambda}(t,\sigma)u(t+\sigma)\mathrm{d}\sigma \end{aligned}$$

$$+ \tilde{k}(t)r(t) \tag{3.16}$$

where $\alpha \triangleq [\ \alpha_1 \quad \alpha_2\ ]$. It is shown in Chapter 2 that the differential equations, (3.9), (3.10), (3.11) together with the control signal (3.16) describe the closed loop dynamics as

$$\begin{aligned}
&\dot{X}_{\mathrm{p}}(t) = A_{\mathrm{m}}X_{\mathrm{p}}(t) + b_{\mathrm{m}}[\tilde{\alpha}^T(t-\tau)\omega(t-\tau) \\
&+ \int_{-\tau}^{0} \tilde{\lambda}(t-\tau,\sigma)u(t-\tau+\sigma)\mathrm{d}\sigma + \tilde{k}(t-\tau)r(t-\tau) + k^*r(t-\tau)], \\
&y_{\mathrm{p}}(t) = h_{\mathrm{m}}^T X_{\mathrm{p}}(t)
\end{aligned} \tag{3.17}$$

where, $X_{\mathrm{p}} \triangleq \left[\ x_{\mathrm{p}}^T \quad \omega_1^T \quad \omega_2^T\ \right]^T$, $h_{\mathrm{m}}^T \triangleq \left[\ h_{\mathrm{p}}^T \quad 0 \quad 0\ \right]$, $y_{\mathrm{p}} = y$ and A_{m} is a constant Hurwitz matrix. From the model matching condition, we know that when the parameter errors are equal to zero, the closed loop transfer function is identical to that of the reference model. Therefore, the reference model can be described by the $(3n)^{\mathrm{th}}$ order differential equation

$$\dot{X}_{\mathrm{m}}(t) = A_{\mathrm{m}}X_{\mathrm{m}}(t) + b_{\mathrm{m}}k^*r(t-\tau),\ y_{\mathrm{m}}(t) = h_{\mathrm{m}}^T X_{\mathrm{m}}(t) \tag{3.18}$$

where,

$$\begin{aligned}
&X_{\mathrm{m}}(t) \triangleq \left[x_{\mathrm{p}}^{*T} \quad \omega_1^{*T} \quad \omega_2^{*T}\right]^T, \\
&h_{\mathrm{m}}^T\left(sI - A_{\mathrm{m}}\right)^{-1} b_{\mathrm{m}}k^* = \frac{k_{\mathrm{m}}}{R_{\mathrm{m}}(s)}.
\end{aligned} \tag{3.19}$$

Note that $x_{\mathrm{p}}^*(t), \omega_1^*(t)$ and $\omega_2^*(t)$ can be considered as the signals in the reference model corresponding to $x_{\mathrm{p}}(t), \omega_1(t)$ and $\omega_2(t)$ in the closed loop system. Therefore, subtracting (3.18) from (3.17), we get an error equation for the overall system as

$$\begin{aligned}
\dot{e}(t) \;=\; & A_{\mathrm{m}}e(t) + b_{\mathrm{m}}[\tilde{\alpha}^T(t-\tau)\omega(t-\tau) \\
& + \int_{-\tau}^{0} \tilde{\lambda}(t-\tau,\sigma)u(t-\tau+\sigma)\mathrm{d}\sigma \\
& + \tilde{k}(t-\tau)r(t-\tau)],
\end{aligned} \tag{3.20}$$

$$e_1(t) = h_{\mathrm{m}}^T e(t).$$

where $e(t) = X_{\mathrm{p}} - X_{\mathrm{m}}$ and $e_1(t) = y_{\mathrm{p}}(t) - y_{\mathrm{m}}(t)$. Equation (3.20) can be written in a more compact form as

$$\begin{aligned} \dot{e}(t) &= A_{\mathrm{m}} e(t) + b_{\mathrm{m}}[\tilde{\theta}^T(t-\tau)\Omega(t-\tau) \\ &\quad + \int_{-\tau}^{0} \tilde{\lambda}(t-\tau,\sigma)u(t-\tau+\sigma)\mathrm{d}\sigma] \\ e_1(t) &= h_{\mathrm{m}}^T e(t). \end{aligned} \tag{3.21}$$

Using the error model (3.21) and defining an appropriate Lyapunov Krasovskii functional, it can be shown [43] that the plant (3.7), adaptive controller and the adaptive laws given in (3.14) have bounded solutions for all $t \geqslant t_0$ and $\lim_{t\to\infty} e_1(t) \to 0$.

3.2.2 Implementation Enhancements

In order to apply the Adaptive Posicast Controller specified by (3.10), (3.11) and (3.14), one has to address several issues which were not taken into account during the initial design but arise in the implementation. Below, we explain these issues and how we address them.

Disturbance rejection

Controller (3.14) is a model reference adaptive controller where the goal is to force the plant output follow the reference model output. In the design stage, the input disturbances are not explicitly taken into account. However, in the idle speed application, it can be shown that the controller is rejecting constant input disturbances. Indeed, the reference, idle speed set-point, is constant, which turns the feed-forward term $k(t)r(t)$ into a pure integrator. Please see Appendix B for the proof of the disturbance rejection.

Approximation of the finite integral term

The finite integral term in the control signal u given in (3.14) is implemented by using a set of point-wise delays [12] as follows:

$$\int_{-\tau}^{0} \lambda(\sigma, t)u(t+\sigma)\mathrm{d}\sigma = \lambda_1(t)u(t-dt) + .. + \lambda_m(t)u(t-mdt) \tag{3.22}$$

where dt is the sampling interval and $mdt = \tau$. In the experiments $dt = 30$ ms, so $m = 0.15/0.03 = 5$. With this approximation, the adaptive laws given in (3.14) can be represented as

$$\dot{\bar{\theta}}(t) = -\bar{\Gamma}e_1(t)\bar{\Omega}(t-\tau) \tag{3.23}$$

where,

$$\bar{\theta} = \begin{bmatrix} \alpha_1 \\ \alpha_2 \\ \lambda_1 \\ \vdots \\ \lambda_m \\ k \end{bmatrix}, \qquad \bar{\Omega} = \begin{bmatrix} \omega_1 \\ \omega_2 \\ u(t-dt) \\ \vdots \\ u(t-mdt) \\ r \end{bmatrix}, \tag{3.24}$$

and $\bar{\Gamma} > 0$ is a diagonal adaptation rate matrix.

In [75], the limitations of this approximation have been pointed out together with an example of unstable behavior arising due to numerical integration. In the power-train control problem considered here, both in the experiments and in the simulations, the values of coefficients λ_i are in the order of 10^{-4}, and for these values we have been able to confirm that the danger of the instabilities due to numerical approximation does not arise. In addition, the stability margin for different values of λ_i's is quite large. See Appendix D for details.

Robustness

The adaptive controller design presented in Section 3.2.1 portrayed an idealized situation. The delay free part of the plant dynamics, $W_p(s)$, is assumed to be finite

dimensional, linear and time invariant with unknown parameters. It is also assumed that the inputs and outputs to the plant can be measured exactly. However, in the real implementation, no plant is truly linear or finite dimensional. Plant parameters may vary with time and operating conditions, and measurements may be contaminated by noise. The plant model is almost always approximate. It is precisely in these cases that adaptive control is most needed [74].

Due to the above possible violations of the assumptions, the controller parameters may drift without converging to a bounded region. One of the remedies to this problem is using a σ-modification robustness scheme [74], which mainly adds a damping term to adaptation laws. With the σ-modification, the adaptive law given in (3.23) is modified as

$$\dot{\bar{\theta}}_{\mathrm{i}}(t) = -\bar{\Gamma}_{\mathrm{ii}} e_1(t) \bar{\Omega}_{\mathrm{i}}(t-\tau) - \sigma \bar{\theta}_{\mathrm{i}}(t) \tag{3.25}$$

where σ is a constant. The drawback of this adaptive law is that the origin is no longer an equilibrium point of (B.5) and (3.25). This implies that even when all the assumptions are perfectly satisfied, the errors do not converge to zero. One way to remedy this drawback is to use a conditional σ-modification scheme:

$$\dot{\bar{\theta}}_{\mathrm{i}}(t) = \begin{cases} -\bar{\Gamma}_{\mathrm{ii}} e_1(t) \bar{\Omega}_{\mathrm{i}}(t-\tau) - \sigma \bar{\theta}_{\mathrm{i}}(t) & \text{if} \quad |\bar{\theta}_{\mathrm{i}}| \geqslant \breve{\bar{\theta}}_i \\ -\bar{\Gamma}_{\mathrm{ii}} e_1(t) \bar{\Omega}_{\mathrm{i}}(t-\tau) & \text{otherwise} \end{cases} \tag{3.26}$$

where, $\breve{\bar{\theta}}_i$ is a predetermined constant. Although we observed in our vehicle experiments that this method is working well for the idle speed control application, one limitation of this method is a lack of automatic procedure to predetermine the value of $\breve{\bar{\theta}}_i$. Several approaches to selecting $\breve{\bar{\theta}}_i$ have been proposed. Firstly, one may fix the value of $\breve{\bar{\theta}}_i$ as the corresponding controller parameter vector which will satisfy the model matching condition for the worst case uncertainty in the plant parameters. Alternatively, some experiments can be conducted without using σ-modification and the controller parameters can be observed after which a reasonable value for the $\breve{\bar{\theta}}_i$ can be selected depending on these observations. For example, one can observe the values of $\bar{\theta}_i$ at different operating points and then select a $\breve{\bar{\theta}}_i$ that prevents the

$\bar{\theta}_i$ drifting away a certain range of these observed values. Finally, another method might be first setting the initial values of the controller parameters in such a way that model matching is satisfied for nominal plant parameters and then $\breve{\bar{\theta}}_i$ can be set as a certain percentage higher than the absolute value of these initial conditions. In our experiments, we used the second proposed method.

Adaptation rate selection

We choose the adaptation gain $\bar{\Gamma}_{\mathrm{ii}}$ for a particular controller parameter $\bar{\theta}_{\mathrm{i}}$ using the following empirical rule

$$\bar{\Gamma}_{\mathrm{ii}} = \frac{\left|(\bar{\theta}_{\mathrm{i}})^*_{\mathrm{e}}\right|}{3\tau_{\mathrm{m}}\left|e_1(t)\bar{\Omega}_{\mathrm{i}}(t-\tau)\right|} \approx \frac{\left|(\bar{\theta}_{\mathrm{i}})^*_{\mathrm{e}}\right|}{3\tau_{\mathrm{m}}(r^*)^2} \tag{3.27}$$

where $(\bar{\theta}_{\mathrm{i}})^*_{\mathrm{e}}$ is an estimate of the desired control parameter, τ_{m} is the time constant of the reference model and r^* is a characteristic value of the reference signal. The rationale for the above is that the desired speed of adaptation is determined by the value that the parameter $\bar{\theta}_{\mathrm{i}}$ must reach in a time $3\tau_{\mathrm{m}}$, which corresponds to the settling time. Since the assumption is that the plant parameters are unknown, the actual desired control parameter vector, $\bar{\theta}^*_{\mathrm{i}}$, is unknown. $(\bar{\theta}_{\mathrm{i}})^*_{\mathrm{e}}$ used in (3.27) should therefore be viewed as an estimate of $\bar{\theta}^*_{\mathrm{i}}$ derived from the matching condition using a nominal plant model. It is assumed that the control parameters start from zero, and also that the orders of magnitude of $e_1(t)$ and $\bar{\Omega}_{\mathrm{i}}(t)$ are close to that of the reference signal. This last assumption can be verified at the first few instants of the operation where the error is approximately equal to the reference signal. So, in a sense, the $\bar{\Gamma}_{\mathrm{ii}}$ selection is based on worst condition where adaptation has just begun.

Fine-tuning

Equations (3.22) and (3.27) imply that $(\bar{\theta}_{\mathrm{i}})^*_{\mathrm{e}}$ and therefore λ^*_{i}, i = 1, 2, .., 15, need to be estimated to determine $\bar{\Gamma}$. Since λ_{i}'s were observed to be small in the simulations, we determined the ideal values of the controller parameters neglecting the delay in the plant and using a pole placement procedure [74]. Also, λ_{i}'s were observed to have

the same order of magnitude for all i, which suggests that the same adaptation gain, $\bar{\Gamma}_\lambda$ for λ_i, $i = 1, .., 5$ can be used in (3.23). The value of $\bar{\Gamma}_\lambda$ was determined using simulation studies of the linearized model.

Due to the approximations discussed above, the resulting $\bar{\Gamma}$ may be non-ideal. Therefore, a weighting matrix M was included as $\bar{\Gamma}_w = \bar{\Gamma}M$ with

$$M = \begin{bmatrix} z_u I_{n\times n} & 0 & 0 & 0 \\ 0 & z_y I_{n\times n} & 0 & 0 \\ 0 & 0 & I_{m\times m} & 0 \\ 0 & 0 & 0 & z_r \end{bmatrix} \tag{3.28}$$

where, z_u, z_y and z_r are constants that are used to fine-tune the adaptation gains. Extensive simulations and experiments on the F-150 test vehicle revealed that setting $z_u = z_r = 1$ and increasing z_y made the system response faster and improved the disturbance rejection performance by decreasing the overshoots and undershoots after introducing/removing the disturbances.

The above discussion implies that the selection of $\bar{\Gamma}$ requires only two free parameters, $\bar{\Gamma}_\lambda$ and z_y that are to be empirically determined.

Anti-windup logic

The actuator, electronic throttle, has its hard limits and the calculated control signal may sometimes exceed these limits, either from below or from above. In the case of idle speed control application, the desired throttle angle is small and thus the saturation may occur due to the control signal hitting the lower limit of the saturation. Consequently, an add-on algorithm needs to be integrated with the controller that prevents the winding up of the integrators resulting from the adaptation laws in (3.14).

We use anti-windup logic where the main goal is to stop the adaptation if the control signal saturates and if the tracking error, $e_1 = y_m - y_p$, is not favorable. Calling the control signal before the saturation block as u and after the saturation as u_{sat}, the anti-windup algorithm can be expressed as in the following.

$$\dot{\bar{\theta}}_i(t) = \begin{cases} 0 & \text{if } u > u_{sat} \text{ and } e_1 < 0 \\ & \text{or} \\ & u < u_{sat} \text{ and } e_1 > 0 \\ -\bar{\Gamma}_{ii} e_1(t) \bar{\Omega}_i(t-\tau) & \text{otherwise} \end{cases} \tag{3.29}$$

The additional tracking error based condition for not suspending the adaptation during saturation improved the speed of the transient response as has been demonstrated in our vehicle experiments.

There are more rigorous anti-windup methods that are specifically developed for adaptive controllers [76]. We plan to apply these methods in our future research.

3.2.3 Final Design and Calibration

A control design that is meant to be used in a mass-production application must be accessible and easy to use by the engineers who actually implement and support the control strategy in production. This is important given that these engineers may not be highly skilled and experienced in advanced control methods. Motivated by these considerations, below we give a step by step design procedure to define a transparent and streamlined design process. We assume that a linear plant model with uncertain parameters and a known time delay is available.

Step 1. Select Λ and l of the signal generators defined in (3.10) and (3.11). These signal generators act like state observers and it is suggested that their eigenvalues are selected much faster than the reference model pole. Note that the Λ-l pair must be controllable.

Step 2. Set the initial value of the controller parameters to zero except for the feedforward term $k(t)$. It is suggested that this parameter is initialized such that $k(0) \in (0, 1)$.

Step 3. Set the time constant of the reference model at least two times faster than that of the nominal plant time constant.

Step 4. Set the adaptation rate matrix Γ according to the algorithm given in (3.27).

Step 5. Adjust the parameter z_y until the highest unmeasured load is rejected according to the requirements. Note that increasing z_y decreases transient excursions, however higher gains might cause undesired oscillations.

Apart from these five steps, the design must be integrated with the robustness scheme presented in (3.26).

Note that the controller needs only about 0.35KB of memory for the data storage and requires less than 83 number of operations per computation cycle. This corresponds to less than $2.8 \cdot 10^3$ floating point operations per second (flops). For conventional ECU's the APC controller uses around 0.028 percent of the total computational power, and that is negligible, especially at idle conditions where ECU is underloaded. Please see Appendix C for the calculation of the memory requirements and computational complexity.

3.3 Simulations

This section presents the simulation results using the nonlinear engine model. We note that the simulation model was available for a similar but not exactly the same engine as used in the experimental vehicle. This difference is not essential since we are using an adaptive control approach.

Figure 3-2 shows the response of the nonlinear engine model to step changes in the idle speed set-point. The adaptation rates were calculated setting M = I. Although the response is sluggish, this figure demonstrates that the rule (3.27) produces reasonable initial estimates for the adaptation rates.

Figure 3-3 shows the response of the nonlinear model to step changes in the idle speed set-point by changing z_y to 220. By changing just this single parameter, the increase in the adaptation gain is attained which provides a much faster yet still well damped response.

All initial conditions for the controller parameters were set to zero except for the

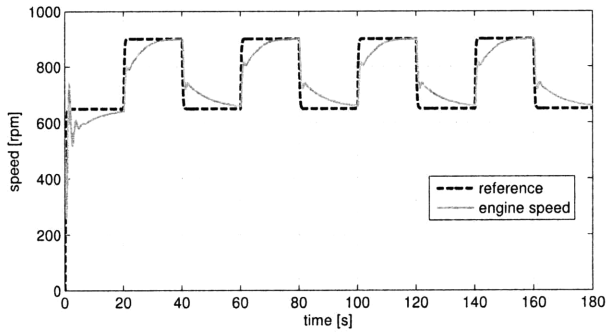

Figure 3-2: Nonlinear model set-point tracking. Adaptation rates are calculated using (3.27) with no further tuning.

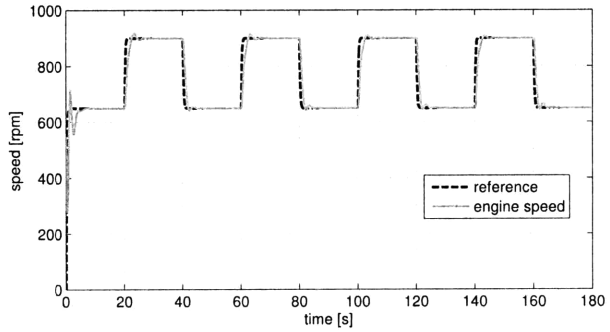

Figure 3-3: Nonlinear model set-point tracking. $z_{\mathrm{u}} = z_{\mathrm{r}} = 1$, $z_{\mathrm{y}} = 220$.

feed-forward term $k(t)$. It was found that any value of $k(0)$ chosen from the interval $(0, 1)$ gave a reasonable performance. Results given in the simulations correspond to the case when $k(0) = 0.3$.

3.4 Experiments

The experimental results given in this section were obtained using an F-150 test vehicle of Ford Motor Company. The vehicle has a 4.6 liter V-8 front engine with a multi-port fuel injection system. The engine has two valves per cylinder and can achieve 231 Hp at 4750 rpm and 397 Nm at 3500 rpm. The air intake is controlled with an electronic throttle.

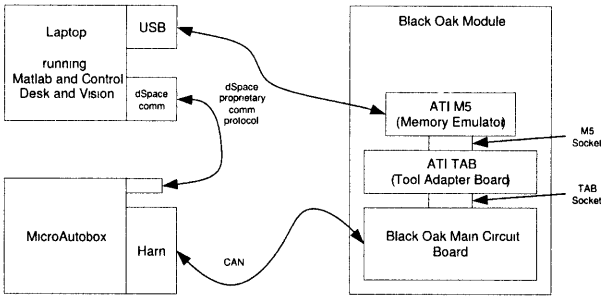

Figure 3-4: Rapid prototyping with MicroAutoBox using CAN.

A dSPACE MicroAutoBox, communicating with the engine control unit (ECU) via CAN bus was used for real-time controller rapid prototyping. This system is used to implement the controller and monitor the performance. Figure 3-4 shows the hardware wiring. In the production environment, the engine is controlled by the ECU. The ECU normally also controls other actuators of the engine, monitors the health of the engine, and processes sensor inputs [77].

In our setup, we override the idle speed control commands coming from the ECU with our adaptive control signal using the rapid prototyping system (see Figure 3-4). This system has the engine speed as the measured input and calculates the throttle command as the control input.

The existing controller on the test vehicle (which we refer to as the baseline controller) consists of a feed-forward controller in parallel with a closed loop controller of PID type. The adaptive controller overrides this feedback controller while the feed-forward controller is retained "as is". Thus our results compare the performance of the existing closed loop controller in the test vehicle with the adaptive controller.

The same adaptation gains used in the simulation shown in Fig. 3-3 were used for all in-vehicle experiments, without further tuning. It was observed that the Adaptive Posicast Controller performed uniformly better when compared to the existing baseline controller, in all experiments.

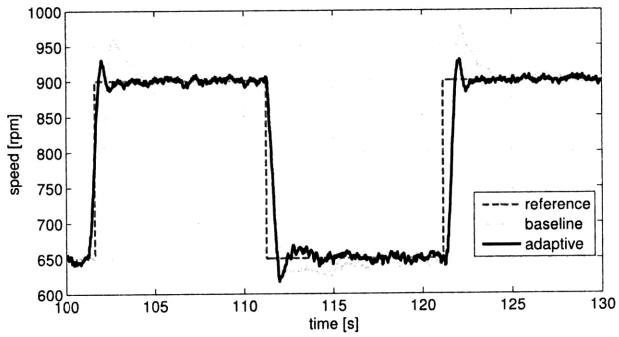

Figure 3-5: Comparison of the baseline controller with adaptive controller for set-point tracking. Γ_w is the same used in the simulation shown in Fig. 3-3

3.4.1 Set-point Tracking

Figure 3-5 shows the set-point tracking performance for both the baseline controller and for the Adaptive Posicast Controller. This experiment was repeated for 3 minutes and the improvement over the baseline controller in RMS error was found to be 6 percent. Note that since most of the time the desired idle speed is constant, the tracking is not the main consideration in idle speed control.

3.4.2 Disturbance Rejection

We next introduced various disturbances into the picture to evaluate the disturbance rejection properties of the Adaptive Posicast Controller. Figure 3-6 shows the deviation from the idle speed (650 rpm) when power steering load is applied repetitively, for two different controllers. The introduction of the disturbance causes the excursions below the set-point and its removal results in the excursions above the set-point. This experiment was conducted for 3 minutes and the RMS error improvement over the existing baseline controller was 35 percent.

In real driving, idle speed set point may change as required to accommodate the states of accessories or changes in the battery voltage. So it is worth comparing the performance of the controllers for different operating points. Figure 3-7 shows the deviation from the idle speed set-point when a power steering disturbance is introduced at 900 rpm, for two different controllers. The dips correspond to the

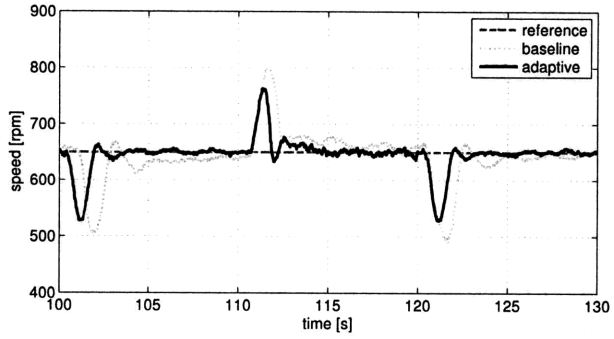

Figure 3-6: Comparison of the baseline controller with adaptive controller for power steering disturbance rejection at 650 rpm. Γ_w is the same as used in the simulation shown in Fig. 3-3

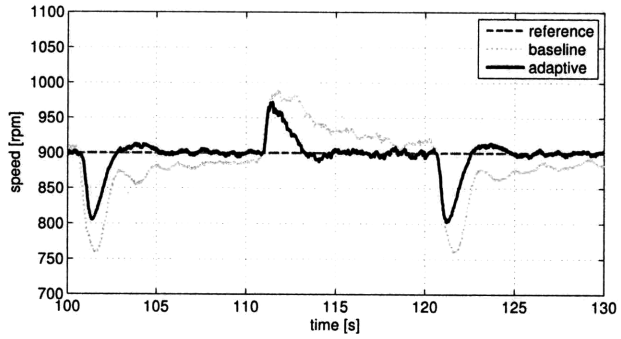

Figure 3-7: Comparison of the baseline controller with adaptive controller for power steering disturbance rejection at 900 rpm. Γ_w is the same as used in the simulation shown in Fig. 3-3

introduction of the disturbance and flares correspond to the release. This experiment was conducted for 3 minutes and RMS error improvement over the existing controller was found to be 48 percent. Similarly, Fig. 3-8 shows the deviation from the idle speed set-point when a power steering disturbance is introduced at 590 rpm, for two different controllers. This experiment was also conducted for 3 minutes and RMS error improvement over the existing controller was found to be 33 percent.

3.4.3 Robustness

Figure 3-9 shows the result of the 3-minute disturbance rejection experiment, a section of which was presented in Fig. 3-6. In the bottom figure of Fig. 3-9 the evolution

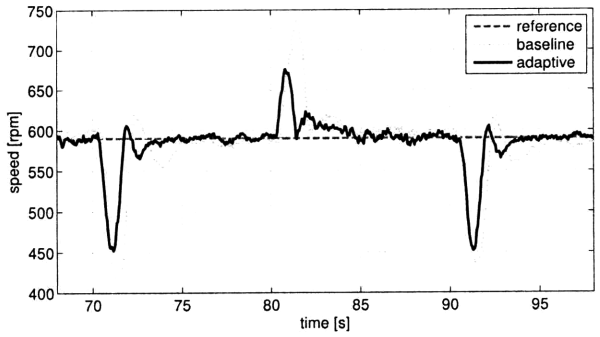

Figure 3-8: Comparison of the baseline controller with adaptive controller for power steering disturbance rejection at 590 rpm. Γ_w is the same used in the simulation shown in Fig. 3-3

of some of the adaptive parameters is presented. Note that the parameters continue to adapt during the course of the experiment and they seem to keep decreasing with a certain slope. As we discussed previously, there may be many reasons for this parameter drift, some of which can be unmodeled dynamics, noise and measurement errors. Another possibility is that the parameters would converge to a bounded region after a long time period. In any case, it is not practical to apply the adaptive controller without a robustness scheme which will make sure that the parameters stay in a predetermined bounded region so that the possibility of instability is avoided.

Figure 3-10 presents the disturbance rejection experimental result where we applied the robustness scheme which is explained in (3.26). Note that the adaptive parameters continue to decrease until they hit their predetermined values and then continue to adapt without leaving that region and stay bounded. An interesting point here is that although the adaptation is restricted in a certain region, the performance improvement is still more or less the same, 38 percent, as in the case without any restrictions (36 percent).

3.5 Summary

We successfully applied the Adaptive Posicast Controller for time-delay systems proposed in [19] and [43] to the idle speed control (ISC) problem in an internal combustion

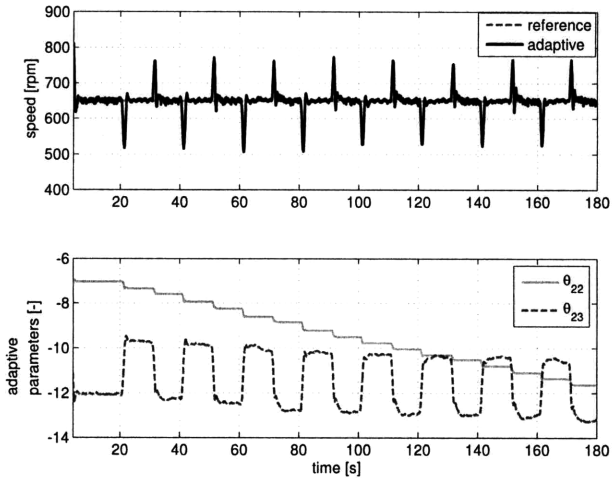

Figure 3-9: Top figure: Adaptive controller performance for power steering disturbance. Bottom figure: Evolution of the controller parameters.

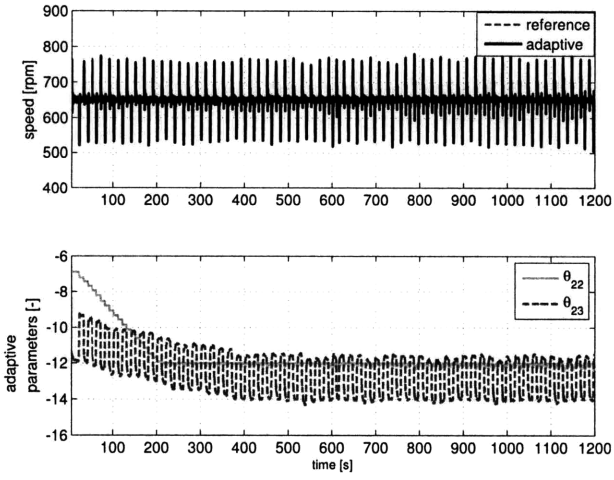

Figure 3-10: Top figure: Adaptive controller performance for power steering disturbance. Bottom figure: Evolution of the controller parameters with σ-modification.

engine. In addition to initial controller design which is presented in section 3.2.1, we enhanced the controller with a robustifying scheme, an adaptation rate selection algorithm, a fine-tuning procedure and an anti-windup logic, and we demonstrated the disturbance rejection properties of the controller. Note that all these enhancements are built hand in hand with the implementation since they all stemmed from the implementation requirements.

Simulations and in-vehicle experimental results confirm that performance improvements can be attained using this approach. In addition, the approach has a potential to reduce calibration time and effort due to two reasons: First, the controller performs better than the existing baseline controller which suggests that the overall controller (feed-forward + closed loop) can be designed by relying less on the feed-forward part which consumes most of the calibration time and effort. Second, the procedure developed in Section 3.2.2 and 3.2.2 dramatically facilitates the design of the adaptive controller and minimizes the tuning process. Hence, the controller can be designed with minimum iteration which means reduced calibration time.

Chapter 4

Spark Ignition Engine Fuel-to-Air Ratio Control: An Adaptive Control Approach

4.1 Plant Model

A block diagram representation of the plant, from fuel injection to the universal exhaust gas oxygen (UEGO) sensor measurement, together with the TWC is shown in Fig. 4-1, where "A" stands for the air charge that is calculated based on the driver torque command. The fuel inducted into the engine cylinders is viewed as the sum of the output of the WW dynamics block and the canister purge, while the fuel injected by the injectors is an input to the WW block. The multiplication by the gain in the "$1/A$" block gives the FAR of the mixture in the engine cylinders (we will consider the control of FAR as opposed to air-to-fuel ratio (AFR) since it scales linearly with fuel) and the delay block represents the combined effect of time delays in the system. The largest contributors to that delay are the time from the fuel injection to exhaust gas formation and the time needed for the exhaust gases to reach the UEGO sensor location. Finally, the exhaust gases undergo mixing, FAR is measured by the UEGO sensor and then the mixture passes through the TWC to get

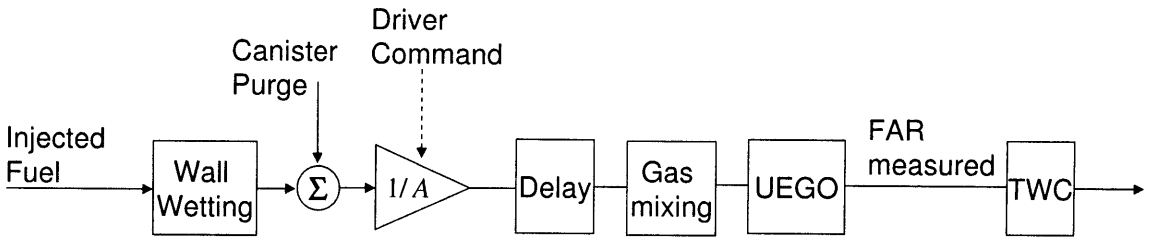

Figure 4-1: Plant block diagram representation.

stripped from its pollutants.

In the model we use, the input is the mass flow rate of fuel injected by the injectors and the output is the equivalence ratio, which is the fuel to air ratio normalized by its stoichiometric value, measured by the UEGO sensor in the exhaust. As explained above, there are mainly four components of the FAR dynamics which are wall-wetting dynamics, fuel-air mixture formation, mixture propagation to the UEGO sensor location and finally UEGO sensor dynamics. Below, the modeling aspects for each component together with their transfer functions are explained.

4.1.1 Wall-Wetting (WW) Dynamics

After the fuel is injected by the injectors, some of the fuel immediately evaporates and is inducted into the engine cylinders, while the rest replenishes a liquid fuel puddle, which forms on the walls of the intake ports and on the intake valves. A fraction of the fuel evaporates from the liquid puddle and is also inducted into the engine cylinders. A WW dynamics model represents this phenomenon with the following transfer function.

$$\frac{F_c(s)}{F_i(s)} = \frac{1 + (1 - X)\tau_{vs}}{\tau_v s + 1} \tag{4.1}$$

where F_c, F_i, X and τ_v represent the fuel entering the cylinders, injected fuel, the fraction of the fuel contributing to the fuel puddle and the puddle evaporation time constant, respectively.

4.1.2 FAR Formation and Propagation to the UEGO Sensor

The vaporized fuel mixes with the air and forms the fuel-air mixture. This process may be modeled as a division of the fuel mass by the air mass, $A(t)$, entering the cylinder. Starting from the opening of the intake valve, it takes approximately one engine cycle, i.e., 2 crankshaft revolutions, until the exhaust gases fully exit the cylinder. This delay is called the cycle delay, τ_c, and can be approximated as $\tau_c = 120/N$, where N is the engine speed in revolutions-per-minute.

After the exhaust gases exit the cylinder, they mix with the previously existing exhaust gases and travel through the exhaust manifold until they reach the UEGO sensor location. Also, in a multi-cylinder engine, the exhaust gases coming from the individual cylinders enter the exhaust manifold at different times. All these effects can be modeled by a pure delay element in series with a first order lag as

$$\frac{\Phi_{bm}(s)}{\Phi_{eng}(s)} = \frac{1}{\tau_{gm}s + 1} e^{-\tau_{tr}} \tag{4.2}$$

where, Φ_{bm}, Φ_{eng}, τ_{gm} and τ_{tr} represent the equivalence ratio, which is fuel-to-air ratio divided by stoichiometric (desired) fuel-to-air ratio, just before the measurement, equivalence ratio right after the engine exit, gas mixing time constant and transport delay, respectively.

4.1.3 Sensor Dynamics

Sensor dynamics can be modeled by a first order lag as

$$\frac{\Phi_m(s)}{\Phi_{bm}(s)} = \frac{1}{\tau_s s + 1} \tag{4.3}$$

where $\Phi_m(s)$ and τ_s represent the measured equivalence ratio and sensor time constant, respectively.

4.1.4 Reduced Order Model

When all the individual elements of FAR dynamics described in eqns. (4.1)-(4.3) are combined, a third order transfer function in series with a pure delay is obtained. To simplify the controller design, a first order lag in series with a pure time delay is used as a reduced order plant model, where the input and the output are the deviations in the commanded in-cylinder equivalence ratio and the measured equivalence ratio.

$$G(s) = \frac{1}{\tau_{\mathrm{m}} s + 1} e^{-\tau s} \tag{4.4}$$

Accurate WW compensation (effectively, the feedforward inversion of (4.1)) helps to render this approximation more valid. Using relay feedback identification method for time delay systems [78] the coefficients of this model at around the speed of 700 rpm and at warm conditions are found to be 0.4 and 0.45 for τ_{m} and τ, respectively. Note that τ consists of the cycle delay τ_{c} and the transport delay τ_{tr} and it also accounts for the UEGO sensor time delay and the computational delay in the engine control unit.

4.2 Controller Design

The structure of the closed loop system used in the test vehicle is presented in Fig. 4-2. The figure shows the inner and the outer control loops. The outer loop determines the desired FAR, $(F/A)_{\mathrm{d}}$, depending on the state of the TWC, measured by the HEGO sensor. $(F/A)_{\mathrm{d}}$ becomes the reference for the inner loop controller or the feedback controller, which is referred to as "Controller". The air estimate, referred to as $\hat{A}$, depends on the driver torque request. The multiplication of $(F/A)_{\mathrm{d}}$ with $\hat{A}$ is referred to as the "base fuel", F_{b}, which is an estimate of the desired fuel. The feedback controller corrects this estimate using the UEGO sensor measurement of the FAR upstream of the TWC. Note that the feedback controller applies a multiplicative correction as opposed to additive correction, although the latter is more typical in controls literature. The advantage of the multiplicative feedback over additive feed-

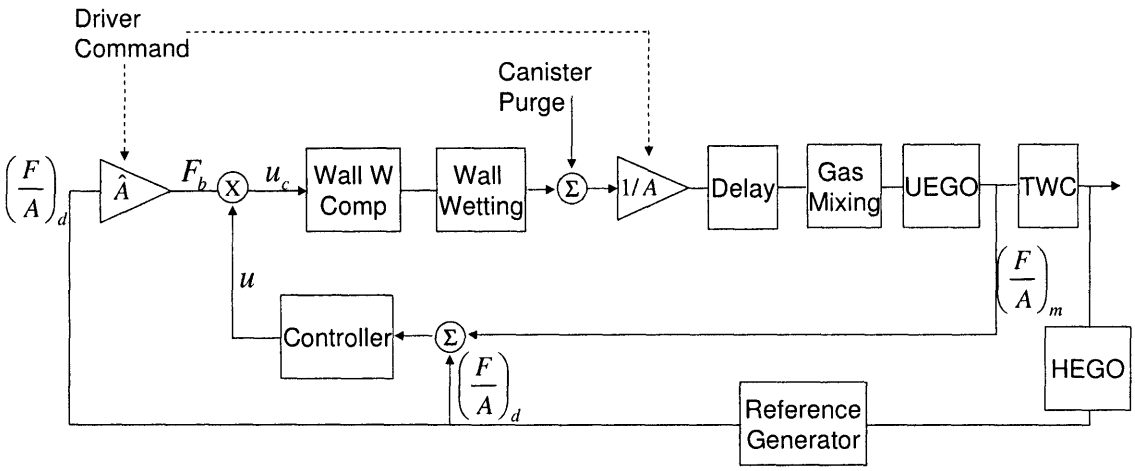

Figure 4-2: Overall closed loop controller structure.

back is that the feedback fuel quantity scales proportionally to the value of the base fuel thereby providing better ability to compensate in transients when changes in vehicle operating point occur. Indeed, this multiplicative transformation maintains the dc gain of the Plant assumed for fuel-to-air ratio feedback design constant across the vehicle operating range. In addition to the feedback controller there is a WW compensation algorithm in the system which estimates the WW dynamics and uses the inverse dynamics to cancel it.

What we are interested in is the feedback controller, for which we design two different adaptive controllers with different complexity. Before explaining these designs, we explain the baseline controller first, which is the existing feedback controller in the vehicle.

4.2.1 Baseline Controller

The baseline controller in the vehicle is essentially a gain-scheduled Proportional-plus-Integral (PI) controller. In the actual vehicle implementation, a first-order filter in series with PI controller and relay logic are used. Note that before the feedback control input is multiplied by the base fuel F_b, it is shifted by 1. So the resulting

control input for the baseline controller can be given as

$$u_c = (1 + u)F_b, \tag{4.5}$$

where u_c is the total control signal without the WW compensation and u is the output of the feedback controller. This structure has the advantage of a feedback control input u that has relatively small values, since it's bias, 1, is already causing the control signal u_c to be equal to the required base fuel F_b.

Note that, to maintain stability in the presence of delay, the gains of the PI controller cannot be made very aggressive. Moreover, due to the delay in the system, the overshoot in the response is difficult to avoid using this feedforward-feedback combination.

4.2.2 Adaptive Feedforward Controller (AFFC)

The system diagram with the Adaptive Feedforward Controller (AFFC) is shown in Fig. 4-3. This is a simple model reference adaptive controller, where it is assumed that the only uncertainty occurs in the control input gain. Instead of the feedback path in Fig. 4-2, a gain multiplier on the $(F/A)_d$ is adapted. Note that the outer loop is not shown in the figure. The motivation for AFFC is to compensate for errors in the base fuel calculation due to, for example, injector uncertainties or "lost-fuel" effects present at cold engine conditions. Assuming that the desired FAR is in general constant and equal to stoichiometric FAR, it can be shown that this controller can also reject constant disturbances.

To derive the adaptation law, consider the following reduced order plant model represented in state space form with a constant disturbance

$$\dot{x}_p = ax_p + b(u(t - \tau) + d) \tag{4.6}$$

where, x_p represents the measured FAR, a and b are known and unknown constants respectively and d is a constant, unknown disturbance. Since the plant is stable, a

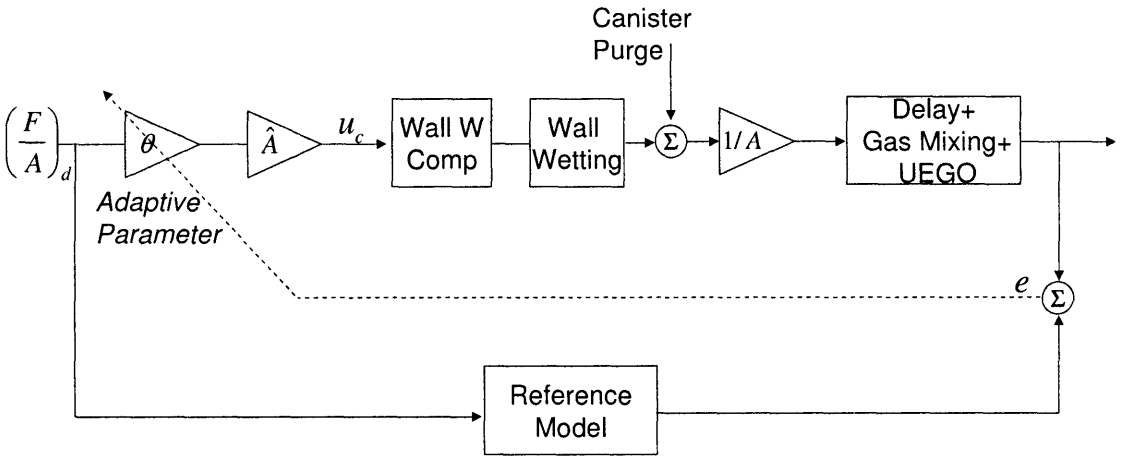

Figure 4-3: Inner-loop structure with AFFC.

is negative and since b represents the gain of the injectors, it is positive. Note that since reduced order dynamics is first order, (4.6) is a scalar differential equation.

Consider a reference model

$$\dot{x}_{\mathrm{m}} = ax_{\mathrm{m}} + b_{\mathrm{m}}r(t-\tau) \tag{4.7}$$

where r is the desired FAR or $(F/A)_{\mathrm{d}}$. Assuming that the reference FAR is constant so that $r = r_0$, we choose the control input as

$$u = \theta r_0 = (\theta^* + \tilde{\theta}(t))r_0 \tag{4.8}$$

where $\theta^* = b_{\mathrm{m}}/b - d/r$ is the ideal controller parameter and $\tilde{\theta}$ is the deviation of θ from θ^*. By using a Lyapunov function candidate $V = (e^2 + b\tilde{\theta}^2)/2$, it can be shown that $\tilde{\theta}(t)$ is bounded and $lim_{t\to\infty}e(t) = 0$, if the following update law is used

$$\dot{\tilde{\theta}} = \dot{\theta} = -\gamma er \tag{4.9}$$

where γ is the adaptation rate and $e = (F/A)_{\mathrm{m}} - (F/A)_{\mathrm{rm}}$. Here $(F/A)_{\mathrm{m}}$ and $(F/A)_{\mathrm{rm}}$

represents the measured FAR and the output of the reference model.

One of the advantages of AFFC is providing a more damped response compared to the baseline controller when the goal is reference tracking. In addition AFFC is easier to tune since it has only one parameter. Note that an adaptation law (4.9) can be enhanced with a dead-band or a sigma-modification and with a projection algorithm.

4.2.3 Adaptive Posicast Controller (APC)

Please see Section 3.2.1 for APC design.

4.2.4 Implementation Enhancements

In order to implement the Adaptive Posicast Controller specified by (3.10), (3.11) and (3.14), one has to address several issues which were not taken into account during the initial design but arise in the implementation. Below, we explain these issues and how we address them.

Disturbance rejection

Controller (3.14) is a model reference adaptive controller where the goal is to force the plant output follow the reference model output. In the design stage, the input disturbances are not explicitly taken into account. However, in the FAR control application, it can be shown that the controller is rejecting constant input disturbances. Indeed, the reference, FAR set-point, is constant for this application, which turns the feedforward term $k(t)r(t)$ into a pure integrator. Please see Appendix B for the proof of the disturbance rejection.

Initialization and Adaptation Rate Selection

We initialize our controller parameters by satisfying the model matching using a nominal plant model. For the nominal plant we choose 700 rpm as the engine speed at warm idling conditions. Idling can be considered as the worst case since the delay

value achieves its maximum value. In this operating condition τ and τ_m is found to be 0.4 and 0.45 respectively.

We choose the adaptation gain $\bar{\Gamma}_{ii}$ for a particular controller parameter $\bar{\theta}_i$ using the following empirical rule

$$\bar{\Gamma}_{ii} = c\bar{\theta}_{i0} \tag{4.10}$$

where c is an adjustable gain and $\bar{\theta}_{i0}$ is the initial value of the corresponding controller parameter. Note that we use the same c for all the parameters which makes the fine tuning procedure easy and fast. The rationale for this rule is to make all the controller parameters equally effective in the control law.

Approximation of the finite integral term

The finite integral term in the control signal u given in (3.14) is implemented by using a set of point-wise delays [12] as in the following:

$$\int_{-\tau}^{0} \lambda(\sigma,t)u(t+\sigma)\mathrm{d}\sigma = \lambda_1(t)u(t-dt) + .. + \lambda_m(t)u(t-mdt) \tag{4.11}$$

where dt is the sampling interval and $mdt = \tau$. With this approximation, the adaptive laws given in (3.14) can be represented as

$$\dot{\bar{\theta}}(t) = -\bar{\Gamma}e_1(t)\bar{\Omega}(t-\tau) \tag{4.12}$$

where,

$$\bar{\theta} = \begin{bmatrix} \alpha_1 \\ \alpha_2 \\ \lambda_1 \\ \vdots \\ \lambda_m \\ k \end{bmatrix}, \qquad \bar{\Omega} = \begin{bmatrix} \omega_1 \\ \omega_2 \\ u(t-dt) \\ \vdots \\ u(t-mdt) \\ r \end{bmatrix}, \tag{4.13}$$

and $\bar{\Gamma}$ is the diagonal adaptation rate matrix.

In [75] the limitations of this approximation have been pointed out together with

an example of unstable behavior arising due to numerical integration. In the power-train control problem considered here, both in the experiments and in the simulations, the values of coefficients λ_i are in the order of 10^{-3} to 10^{-4}, and for these values the danger of the instabilities due to numerical approximation does not arise.

Handling Time-Varying Delay

In the design of the APC, it assumed that the time delay in the system is known and constant. However, the time delay in the FAR control problem varies with the load and the speed of the engine. A logical way of handling this issue is gain-scheduling the controller, time delay being the gain-scheduling variable. The delay value shows itself in the equation (3.10) and in the adaptation laws given in (3.14), which are straightforward to gain-schedule. Apart from these, the finite integral term in the control law given in (3.14) also needs the delay information to be computed. Note that we use an approximation for this term given in (4.11). We pursued two different strategies to gain-schedule this approximation, which are given below:

a) Eliminating and Adding Terms:

The integral in (4.11) is approximated using time steps that are equal to the sampling interval, T, of the controller implementation (T = 30 ms). Therefore, the number of the terms, m, in this approximation can be given as $m = \tau/T$. A simple way to gain-schedule this approximation is to eliminate or add terms, depending on the value of the delay at the time of approximation. One can do this by storing the values of eliminated parameter λ_i's when the delay decreases and then using these stored values when the number of the terms increases again, due to a delay increase.

Although this logic seems intuitive, it has a drawback of rapid control signal changes that can cause undesired excursions in the FAR trace.

b) Freezing and Adding Terms:

As we discussed above, when the delay value decreases, we need less parameters to approximate the finite integral in (4.11) and thus we eliminate the unnecessary terms. This causes a sudden, undesired jump in the control signal. To prevent this jump, instead of eliminating the unnecessary terms, $\lambda_i(t)u(t-idt)$'s, we simply freeze

them and use them back when the delay value increases. This strategy achieves two things: First, it still makes sure that only the necessary terms are being used and thus only the necessary parameter λ_i's are being updated, while the rest of them are frozen. Second, by still keeping the frozen terms in the control signal, it leads a smooth transition from one delay approximation to another.

Note that in the case of a delay decrease and thus freezing of the unnecessary terms, the control signal carries the frozen terms as a constant bias. Below, we show that this does not adversely effect the stability of the closed loop system.

Assume that the delay value τ decreased to $\tau^{'}$ so that we need only need $p = \tau^{'}/T$ terms instead of m terms to approximate the finite integral, where $p < m$. In this case, we freeze the $m - p$ unnecessary terms. Assume that the sum of these frozen terms are equal to D. The resulting approximation is the following:

$$\int_{-\tau^{'}}^{0} \lambda(\sigma, t)u(t+\sigma)\mathrm{d}\sigma = \lambda_1(t)u(t-dt) + .. + \lambda_p(t)u(t-pdt) + D. \tag{4.14}$$

The state space description of the plant together with the controller given in (2.31) is now modified as

$$\dot{x}_\mathrm{p}(t) = A_\mathrm{p}x_\mathrm{p}(t) + b_\mathrm{p}(u(t-\tau) + D), \;\; y(t) = h_\mathrm{p}^T x_\mathrm{p}(t). \tag{4.15}$$

We can, therefore, use the same procedure explained in Appendix B to show that the overall system stays stable and that the tracking error goes to zero.

Anti-windup logic

The fuel injector actuators, have their hard limits and the calculated control signal may sometimes exceed these limits, either from below or from above. Consequently, an add-on algorithm needs to be integrated with the controller that prevents the winding up of the integrators resulting from the adaptation laws in (3.14).

We use anti-windup logic where the main goal is to stop the adaptation if the control signal saturates and if the tracking error, $e_1 = y_\mathrm{m} - y_\mathrm{p}$, is not favorable.

Calling the control signal before the saturation block as u and after the saturation as u_{sat}, the anti-windup algorithm can be expressed as in the following.

$$\dot{\bar{\theta}}_{\text{i}}(t) = \begin{cases} 0 & \text{if } u > u_{\text{sat}} \text{ and } e_1 < 0 \\ & \text{or} \\ & u < u_{\text{sat}} \text{ and } e_1 > 0 \\ -\bar{\Gamma}_{\text{ii}} e_1(t) \bar{\Omega}_{\text{i}}(t-\tau) & \text{otherwise} \end{cases} \tag{4.16}$$

The additional tracking error based condition for not suspending the adaptation during saturation improved the speed of the transient response as has been demonstrated in our vehicle experiments.

There are more rigorous anti-windup methods that are specifically developed for adaptive controllers [76]. We plan to apply these methods in our future research.

Robustness

The adaptive controller design presented in Section III-C portrayed an idealized situation. The delay free part of the plant dynamics, $W_{\text{p}}(s)$, is assumed to be finite dimensional, linear and time invariant with unknown parameters. It is also assumed that the inputs and outputs to the plant can be measured exactly. However, in the real implementation, no plant is truly linear or finite dimensional. Plant parameters may vary with time and operating conditions, and measurements may be contaminated by noise. The plant model is almost always approximate. It is precisely in these cases that adaptive control is most needed [74].

Due to the above possible violations of the assumptions, the controller parameters may drift without converging to a bounded region. One of the remedies to this problem is using σ- modification robustness scheme [74], which mainly adds a damping term to adaptation laws. We previously used this robustness scheme in idle speed control application [79] which proved successful and therefore we used it again in FAR control application. Please see [79] for the details.

4.2.5 Final Design and Calibration

We believe that any controller design that is meant to be used in a mass-production application must be accessible and easy to use by the engineering staff who actually implements and supports the control strategy in production. This is particularly important given that the engineering stuff are not expected to be highly skilled in advanced control methods. Motivated by these facts, below we give a step by step design procedure to obtain a transparent and streamlined design. We assume that a linear plant model with uncertain parameters and a known time delay is available.

Step 1. Select Λ and l of the signal generators defined in (3.10) and (3.11). These signal generators act like state observers and it is suggested that the eigenvalues are selected much faster than the reference model pole. Note that the Λ-l pair must be controllable.

Step 2. Set the initial value of the controller parameters by satisfying the model matching using a nominal plant model.

Step 3. Set the time constant of the reference model at least two times faster than that of the nominal plant time constant.

Step 4. Set the adaptation rate matrix Γ according to the algorithm given in (3.27).

Step 5. Tune the parameter c until the control requirements are satisfied. Note that increasing c gives a tighter FAR control performance, however higher gains might cause undesired oscillations.

Apart from these five easy steps, the design must be integrated with the robustness scheme as discussed in Section III-D-6.

Note that the controller needs only about 0.4KB of memory for the data storage and requires 118 number of operations per computation cycle. This corresponds to less than $4 \cdot 10^3$ operations per second. For conventional ECU's the APC controller use around 0.04 percent of the total computational power and that is negligible. Please see

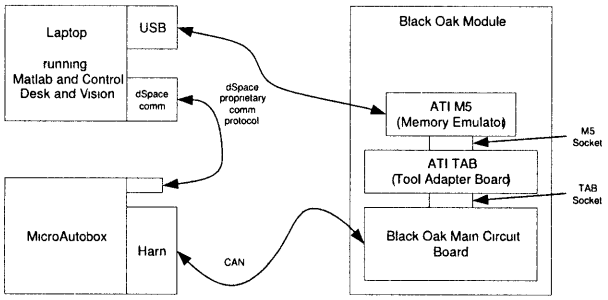

Figure 4-4: Rapid prototyping with MicroAutobox using CAN.

Appendix C for the calculation of the memory requirements and computational complexity for the idle speed control application, which explains the calculation method that is also used for the FAR control implementation.

4.3 Simulation and Experimental Results

The simulation results in this section are obtained using ®Matlab and ®Simulink, and the experimental results are obtained using a Lincoln Navigator test vehicle provided by Ford Motor Company. The vehicle has a 5.4 liter V-8 front engine with a multi-port fuel injection system. The engine has three valves per cylinder and can achieve 300 Hp at 5000 rpm and 495 Nm at 3750 rpm. The air intake is controlled with an electronic throttle.

A dSPACE MicroAutoBox, communicating with the engine control unit (ECU) via CAN bus was used for real-time controller rapid prototyping. This system is used to implement the controller and monitor the performance. Figure 4-4 shows the hardware wiring. In the production environment, the engine is controlled by the ECU. The ECU normally also controls the other actuators of the engine, monitors the health of the engine and processes sensor inputs [77].

In our setup, we override the FAR control commands coming from the ECU with our adaptive control signal using the rapid prototyping system (see Figure 3-4). This system has the FAR as the measured input and calculates the fuel mass flow rate as

the control input.

The existing closed loop control structure in the vehicle is presented in Fig. 4-2. The adaptive controller overwrites the "Controller" block, while the rest of the structure is retained as is. Thus, our results compare the performance of the existing feedback controller in the test vehicle with the adaptive controller. It was observed that the Adaptive Posicast Controller performed better when compared to the existing baseline controller, in all experiments.

4.3.1 AFFC vs. Baseline Controller

Figure 4-5 compares the tracking and purge disturbance rejection performance of the baseline controller and of the AFFC when WW dynamics are assumed to be perfectly compensated. Φ denotes the normalized FAR or the equivalence ratio (so that stoichiometric FAR of 0.0685 corresponds to $\Phi = 1$. The upper plot shows the simulated response to a pulse train reference and the lower plot shows the response to a step purge disturbance introduced at time $t = 30$ sec and removed at time $t = 50$ sec. It is assumed that the time delay is known to be 0.4 sec. While designing the AFFC, the UEGO dynamics are assumed to have nominal values but then the plant dynamics were chosen to have 20 percent deviations in high frequency gain and τ_m. The baseline controller is tuned to perform well for both tracking and disturbance rejection. As discussed before, the baseline controller cannot avoid overshoots due to the delay in the system, while the AFFC can track the reference comparatively better. On the other hand, the disturbance rejection capabilities are similar, since when the reference is constant, the AFFC is essentially an integral controller.

We have also tested AFFC experimentally and compared it with the existing baseline controller. At the test time, the calibration of WW compensation was not fully completed, which allowed to subject both controllers to challenging scenarios. Also, the time delay varied in the experiments as opposed to the cases simulated in Fig. 4-5. Figure 4-6 shows the results from a 4-minute drive test. Note that the air charge values have been scaled to show them in the same plot with Φ. The test was conducted in a relatively uncontrolled environment, e.g., without controlling the

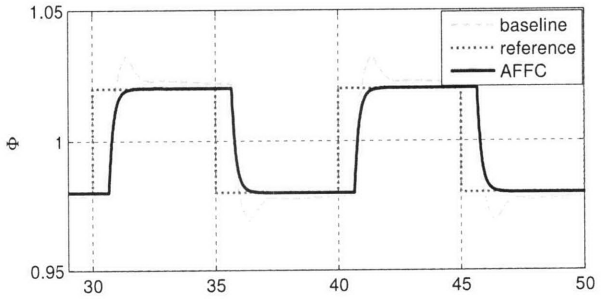

(a)

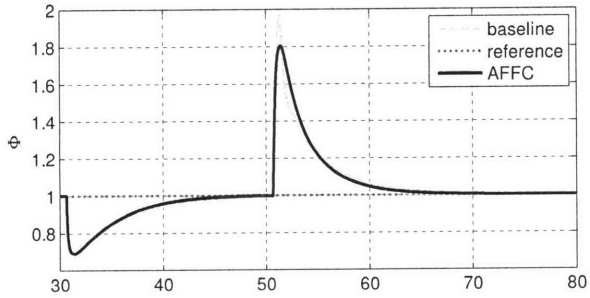

(b)

Figure 4-5: Comparison of baseline controller and AFFC. a) Response to a set-point change b) Response to purge disturbance.

speed or load, as can be observed in Figs. 4-6a-c. The vehicle was accelerated and decelerated rather sharply and the purge flow was also not controlled, as shown in Fig. 4-6-d. The RMS error value of the deviations from the reference is calculated as 0.0052 and 0.0051 for the baseline controller and for the AFFC, respectively. Their performances are similar, consistently with our simulation results, as the dominant factors affecting the response are the purge and air disturbances, and not the reference tracking.

Note that another important success measure (SM) for the FAR control loop is the error integral. Compared to RMS error, this metric better reflects how much of the TWC oxygen storage capacity is used to compensate for the deviations in the fuel-to-air ratio.

The integral error SM can be formulated as

$$\mathrm{SM} = \frac{1}{k}\sum_{i=1}^{k}\left|\int_{t_i}^{t_i+\Delta_i} e_1(\eta)\mathrm{d}\eta\right| \tag{4.17}$$

where t_i is the time instant of the i-th disturbance hit and Δ_i is the duration/settling time of the transient caused by the disturbance hit. We use this SM for the APC results in the following sections.

4.3.2 APC vs. Baseline Controller

Purge Disturbance Rejection Tests

The purpose of our initial FAR control experiments was to compare the performances of the APC and the baseline controller, while emulating canister vapor purge disturbance rejection tests. These experiments were conducted with the test vehicle idling at different speeds. Since during idling the air flow rate does not change much, the WW dynamics did not play a major role in these experiments as much as it did for acceleration and deceleration experiments. The SM used is given in (4.17).

The test started with the engine speed at 700 rpm. At 300 sec, the engine speed increased to 1000 rpm and at 600 sec it decreased back to 700 rpm. Every 20 sec the fuel injector gains were changed to emulate the purge disturbance. Overall, the

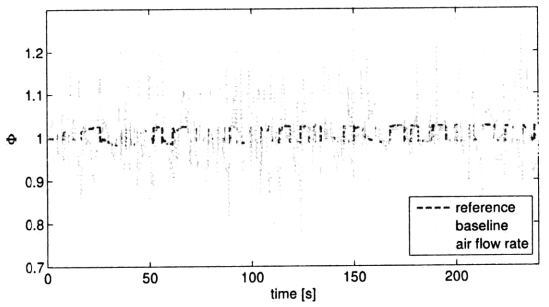

(a)

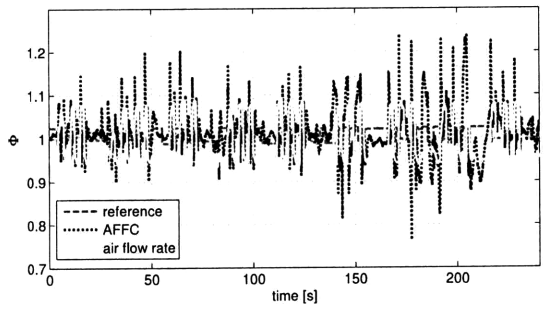

(b)

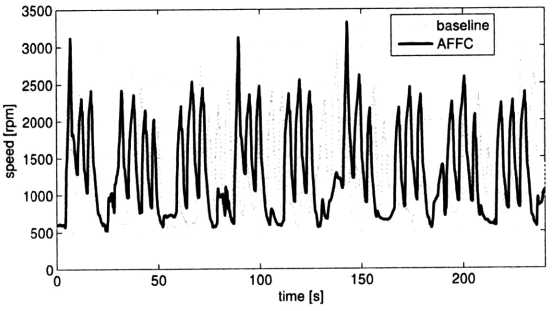

(c)

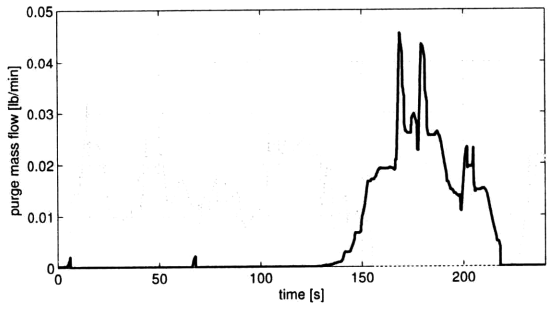

(d)

Figure 4-6: Baseline controller vs. AFFC a) Φ and air flow rate when baseline controller is active b) Φ and air flow rate when AFFC is active c) Engine speeds d) Purge fuel flow rates.

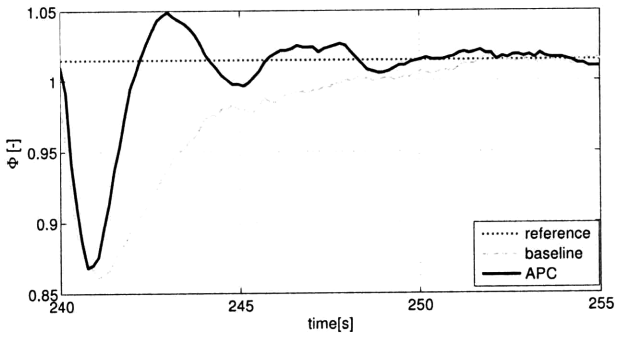

Figure 4-7: Comparison of baseline controller with APC for purge disturbance rejection at 700 rpm.

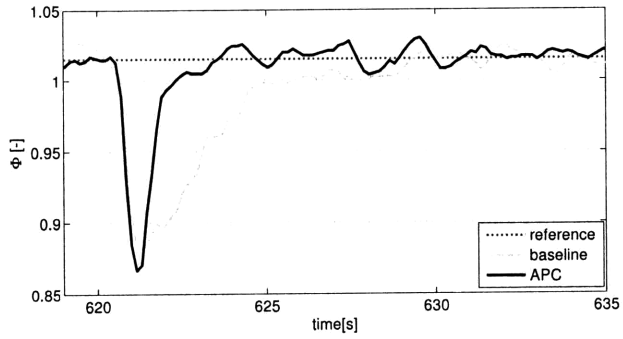

Figure 4-8: Comparison of baseline controller with APC for purge disturbance rejection at 1000 rpm, with $c = 1$.

performance of the APC, calculated using (4.17), was 70 percent better than the baseline controller during the test which lasted 15 minutes. Figure 4-7 shows a time window from the test where the engine speed was 700 rpm. The APC performs considerably better, in terms of integral SM, than the baseline controller as its features enable it to better account for the delay and achieve faster response.

Figure 4-8 shows how the equivalence ratio changes during the same test but now the engine speed is 1000 rpm. Again, the performance of the APC is better than that of the baseline controller.

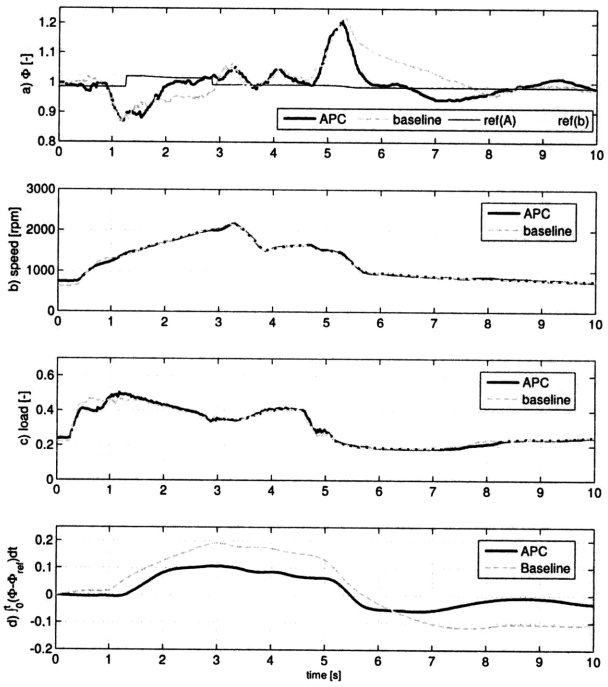

Figure 4-9: Time histories of a) Φ, b) Engine speed c) Engine relative air flow, d) Tracking error integral, during vehicle acceleration and deceleration for APC vs. baseline controller, with $c = 1$.

Acceleration and Deceleration Tests

Figure 4-9 shows the equivalence ratio excursions during a test in which the vehicle accelerates and then decelerates. In this case, the delay varies with time during the test. The APC performs better overall than the baseline controller. During the lean excursion (equivalence ratio less than 1 during acceleration), the baseline controller appears to start the recovery from the undershoot slightly earlier than the APC. There are, however, differences in the air flow and the equivalence ratio set-point time of increase between APC test and baseline controller test, further analysis of these suggests no real advantage for the baseline controller over APC in terms of start of recovery timing. Note that the equivalence ratio set-point is computed by a separate part of the engine control system in the vehicle.

For this experiment, we compared the maximum value of the integrated difference between fuel-air equivalence ratio and its set point during the full course of the exper-

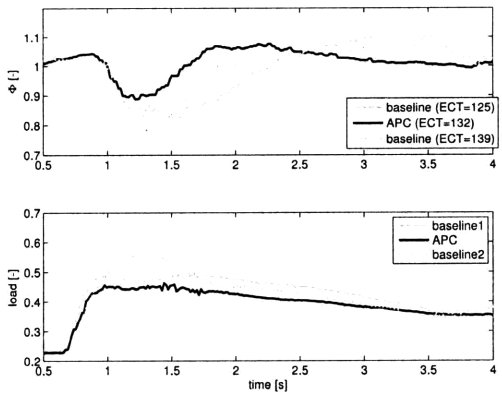

Figure 4-10: Comparison of baseline controller with APC during vehicle acceleration, with $c = 1.5$.

iment. This metric is better suited to assessing the difference between controllers for this experiment than (4.17) because if one acceleration-deceleration test is assumed to be a single event, the errors cancel each other if (4.17) is used, which can be observed in (4-9)-d. However, maximum value of the integral relates to how much of the oxygen storage capacity is used in the worst case during the course of the experiment. In terms of this metric, APC performs 43 percent better than the baseline controller.

All the above experiments were conducted with the fine tuning parameter c equal to 1, which implies that no fine-tuning was done. In Fig. 4-10, we present an experimental result, which shows APC and the baseline controller performances during the vehicle acceleration, with $c = 1.5$. As expected, the APC outperforms the baseline controller to a greater extent compared to the previous cases, especially on lean excursions. Note however that the load (and hence the air charge) are less in the APC controller case in this experiment. Nevertheless, performance with the APC is considerably better than with the baseline controller, and cannot be attributed to the load difference between the controllers.

4.3.3 APC vs. Gain-Scheduled Smith Predictor

We compared the performance of the APC with a gain-scheduled Smith Predictor (SP). The SP was designed based on the plant models identified at different operating points (corresponding to different combinations of engine speeds and loads) using a relay feedback method.

Figure 4-11 shows the results of an acceleration-deceleration test conducted using the test vehicle. The performances are very similar as can be seen in Fig. 4-11a and Fig. 4-11d, where the time evolutions of Φ and the error integral is presented. On the other hand, Fig. 4-11c shows that the control signal of the APC is smoother than that of the SP.

Figure 4-11 confirms that the adaptive controller is performing very well and similar in performance to the Smith Predictor. Note that the gain-scheduled SP can be seen as a perfect adaptive controller: While the APC *adapts* to operating point changes without the knowledge of the plant parameters, the gain-scheduled SP *uses* the knowledge of the changing plant parameters that need to be obtained offline by using an identification procedure for different operating points. The adaptive controller can, in addition, adjust better to situations when plant parameters change due to part-to-part variability or aging. For example, it is stated in [49] that due to aging or harsh operating conditions, UEGO sensor time constant can easily increase by a factor of 10 to 20. Also it is known that the Smith Predictor is sensitive to the delay estimation errors.

In Fig. 4-12, we present the simulation results that compare SP with APC. For this simulation, the time constant for the first order system model is selected as 50 ms, which is reported in [49] as the time constant of a state-of-the-art oxygen sensor. The nominal time delay is assumed to be 0.4 seconds. A step input disturbance is introduced to this plant at time $t = 170$ seconds and the transients are plotted. The APC and the SP is tuned such that they perform similarly for these nominal plant parameter values, in the presence of the disturbance. Then, the sensor time constant is increased by a factor of 20 and the disturbance test is repeated. As seen in the

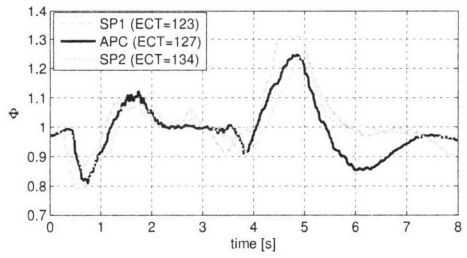

(a)

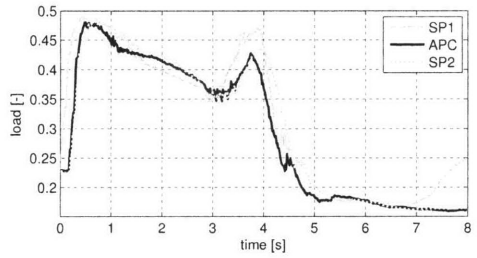

(b)

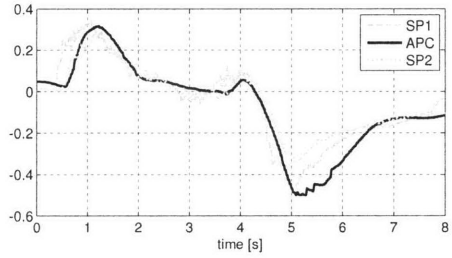

(c)

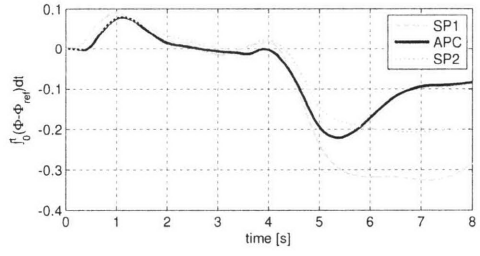

(d)

Figure 4-11: Time histories of a) Φ b) Engine relative air flow c) Feedback control input d) Tracking error integral, during vehicle acceleration and deceleration for gain-scheduled SP vs. APC, with $c = 1.5$.

figure, not only the performance of the SP gets worse than the adaptive controller, but the SP response also becomes oscillatory, which is a sign of getting closer to instability. An additional uncertainty in the system, like a delay identification error, may cause the system to become unstable easily. Indeed, when we introduce a delay uncertainty by increasing the nominal delay by 0.3 seconds, we see that the loop with the SP becomes almost marginally stable. This simulation result is presented in Fig 4-13.

4.4 Summary

In this chapter, we have considered the fuel-to-air ratio (FAR) control problem in port-fuel-injection (PFI) spark-ignition (SI) engine. Two controllers, an Adaptive FeedForward Controller (AFFC) and an Adaptive Posicast Controller (APC), have been developed and implemented in a test vehicle. The AFFC is a simple controller based on feedforward adaptation, while the APC is a more elaborate controller that uses adaptation in both feedforward and feedback paths and is based on a recently developed adaptive control method for time-delay systems. The AFFC has been shown in simulations and experiments to have better reference tracking and similar disturbance rejection capabilities when compared to the existing baseline controller. The APC has been shown in experiments to achieve faster recovery from disturbances and better performance during vehicle acceleration deceleration tests. These performance improvements were a result of various modifications and enhancements to the initial APC design, such as an algorithm to handle the variable time delay, a robustness scheme and parameter initialization and fine tuning methods. It has also been observed in our vehicle experiments that implementing APC using an upper bound on the delay as a delay estimate assures robustness against delay variations.

In terms of applications of the APC, the FAR control problem is more challenging than the Idle Speed Control (ISC) problem, due to a larger and variable time delay and different character of disturbances and uncertainties. The experimental results reported here demonstrate that the APC is effective for the FAR control problem as

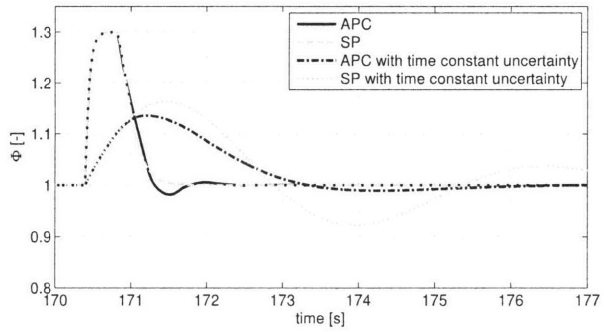

Figure 4-12: Comparison of SP and APC for input step disturbance rejection in the presence of sensor time constant uncertainty.

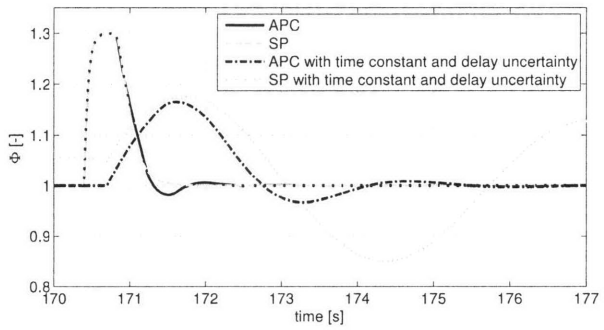

Figure 4-13: Comparison of SP and APC for input step disturbance rejection in the presence of sensor time constant and delay uncertainty.

well.

Chapter 5

Summary and Future Research

In this thesis, the Adaptive Posicast Controller is proposed, which addresses the key challenges due to uncertainties and time delay, that are important for many industrial control applications. It is an adaptive controller with explicit delay compensation built upon the ideas of the classical Smith Predictor, finite spectrum assignment and adaptive control. The main difference of the APC from the earlier designs is that it is easily implementable and computationally affordable. This makes the APC a good candidate for mass production applications like automotive internal combustion engine control.

In this research, the proposed APC has been applied to Idle Speed Control (ISC) and Fuel-to-Air Ratio (FAR) control of automotive engines. The treatment of implementation aspects, including adaptation rate selection, parameter initialization, anti-windup implementation, handling parameter drift and handling time-varying delay is discussed.

In ISC, the objective is to regulate the engine speed to a prescribed set-point in the presence of various load torque disturbances due to power steering, air conditioning, transmission engagement and powering the alternator. In FAR control, the objective is to maintain the in-cylinder fuel-to-air ratio at a prescribed set point, determined primarily by the state of the Three-Way Catalyst (TWC), so that the pollutants in the exhaust are removed with the highest efficiency. The FAR controller must also reject disturbances due to canister vapor purging and inaccuracies in air charge estimation

and wall wetting compensation.

A high performing and robust ISC is important for minimizing fuel consumption, avoiding engine stalls and satisfying NVH (Noise, Vibration and Harshness) requirements. Many challenges to ISC are due to changing operating conditions, uncertainty in the crankshaft load estimation, part-to-part variability and aging. For instance, engine coolant temperature, ambient temperature, humidity, barometric pressure, and fuel type can vary during vehicle operation and components, such as an electronic throttle, can change their characteristics. The idle speed set-point may change depending on the state of transmission, engine or accessories. The induction to power (IP) delay presents another significant challenge to ISC. This delay can be assumed to be constant as it mainly depends on engine speed which does not change significantly during idling.

A high performing and robust FAR control is critical for many vehicle attributes, including emissions, drivability and fuel economy. Note also that the cost of after-treatment system depends on the size and precious metal loading of the TWC which determine its oxygen storage capacity. Whenever there is a deviation of the exhaust fuel-to-air ratio from the stoichiometry, either the excess oxygen is stored in the TWC, or the lack of oxygen is compensated by the use of existing oxygen in the TWC. Therefore, if the fuel-to-air ratio excursions and their durations are reduced with a well-performing controller, the storage capacity of TWC and its cost may be reduced as well. Similar to ISC, changing operating conditions, part-to-part variability, component aging and the time delay present significant challenges to FAR control. Unlike ISC, the delay is time-varying in FAR control case because FAR controller must function across full engine operating range.

All the experimental results presented in this thesis show that the APC performs better than the existing baseline controller in the test vehicles. In addition, it is experimentally verified that the APC works as well as a gain scheduled Smith Predictor, which could be viewed as a perfect adaptive controller for time delay systems. Note that, the APC does not need accurate plant models and it can better compensate the modeling errors and parameter variations due to aging, than the Smith Predictor.

It is also noted that the APC idea can potentially be extended to nonlinear systems, given that suitable Lyapunov-Krasovsky functionals are found. This extension can be explored further as one of the future research directions.

Appendix A

The Bound on the Series S

Defining $a \triangleq c_0^2(t - t_i')$ and $S' \triangleq \sum_{n=1}^{\infty} \left(\frac{a^n}{n!}\right)^{1/2}$, we obtain that

$$S = \left(\bar{f} + c_0 c_1\right) S' \tag{A.1}$$

Summing up the odd terms of S' we have that

$$\begin{aligned} S_o' &= \sqrt{a} + \sqrt{\frac{a^3}{3!}} + \sqrt{\frac{a^5}{5!}} + ... \\ &= \sqrt{a} + a\sqrt{\frac{a}{3!}} + \frac{a^2}{2!}\sqrt{\frac{a}{30}} + ... \end{aligned} \tag{A.2}$$

If $a < 1$, then we obtain that

$$S_o' \leqslant 1 + a + \frac{a^2}{2!} + ... = e^a \tag{A.3}$$

If $a > 1$, then we obtain that

$$\begin{aligned} S_o' &\leqslant a + \frac{a^2}{2!}\frac{1}{\sqrt{1.5}} + \frac{a^3}{3!}\frac{1}{\sqrt{10/3}} + ... \\ &\leqslant 1 + a + \frac{a^2}{2!} + \frac{a^3}{3!} + ... \\ &= e^a. \end{aligned} \tag{A.4}$$

Summing up the even terms, we have

$$\begin{aligned} S_e' &= \frac{a}{\sqrt{2!}} + \frac{a^2}{\sqrt{4!}} + \frac{a^3}{\sqrt{6!}} + \ldots \\ &\leqslant 1 + a + \frac{a^2}{2!} + \frac{a^3}{3!} + \ldots \\ &= e^a \end{aligned} \tag{A.5}$$

Using (A.1), (A.3), (A.4) and (A.5) we obtain that

$$\begin{aligned} S &= \left(\bar{f} + c_0 c_1\right)\left(S_o' + S_e'\right) \\ &\leqslant 2\left(\bar{f} + c_0 c_1\right) e^a. \end{aligned} \tag{A.6}$$

Finally, substituting the definition of a in (A.6) we have

$$S \leqslant 2\left(\bar{f} + c_0 c_1\right) e^{c_0^2 (t - t_i')}. \tag{A.7}$$

This completes the proof.

Appendix B

Disturbance Rejection Proof

When there is a constant disturbance $d \in \Re$ present in the system, the state space description of the plant (2.31) is modified as

$$\dot{x}_{\mathrm{p}}(t) = A_{\mathrm{p}} x_{\mathrm{p}}(t) + b_{\mathrm{p}}(u(t-\tau) + d), \;\; y(t) = h_{\mathrm{p}}^T x_{\mathrm{p}}(t) \tag{B.1}$$

This, in turn, modifies the error equation (3.20) as

$$\begin{aligned} \dot{e}(t) &= A_{\mathrm{m}} e(t) + b_{\mathrm{m}}[\tilde{\alpha}^T(t-\tau)\omega(t-\tau) \\ &\quad + \int_{-\tau}^{0} \tilde{\lambda}(t-\tau,\sigma)u(t-\tau+\sigma)\mathrm{d}\sigma \\ &\quad + \tilde{k}r(t-\tau) + d] \\ e_1(t) &= h_{\mathrm{m}}^T e(t). \end{aligned} \tag{B.2}$$

Note that in idle speed application, the idle speed reference, $r_0 \in \Re$, is constant and, therefore, we have $r(t-\tau) = r_0$ in (B.2). We define a new variable $\tilde{k}'$ as

$$\tilde{k}' = \tilde{k} + \frac{d}{r_0} \tag{B.3}$$

Hence, (B.2) reduces to

$$\begin{aligned} \dot{e}(t) &= A_{\mathrm{m}} e(t) + b_{\mathrm{m}}[\tilde{\alpha}^T(t-\tau)\omega(t-\tau) \end{aligned}$$

$$
\begin{aligned}
&+ \int_{-\tau}^{0} \tilde{\lambda}(t-\tau,\sigma)u(t-\tau+\sigma)\mathrm{d}\sigma \\
&+ \tilde{k}' r_0] \\
e_1(t) &= h_{\mathrm{m}}^T e(t).
\end{aligned} \tag{B.4}
$$

which can also be written as

$$
\begin{aligned}
\dot{e}(t) &= A_{\mathrm{m}} e(t) + b_{\mathrm{m}}[\tilde{\theta}'^T(t-\tau)\Omega(t-\tau) \\
&\quad + \int_{-\tau}^{0} \tilde{\lambda}(t-\tau,\sigma)u(t-\tau+\sigma)\mathrm{d}\sigma] \\
e_1(t) &= h_{\mathrm{m}}^T e(t).
\end{aligned} \tag{B.5}
$$

where, $\tilde{\theta}' = \begin{bmatrix} \tilde{\alpha}_1 & \tilde{\alpha}_2 & \tilde{k}' \end{bmatrix}^T$. Equations (B.5) and (B.2) are exactly the same equations written using different variables, meaning that the definition of the new variable does not alter the equilibrium position of the differential equation. In addition, (B.5) is in the same form as in the case of disturbance free system (3.21), so the stability proof follows the same lines and $\lim_{t\to\infty} e_1(t) \to 0$. So, the system is stable, the disturbance is rejected and the plant output follows the reference model output asymptotically.

To conclude, disturbance rejection is achieved by eliminating the disturbance term in the error equation and this is done by introducing a new variable defined by shifting the feed-forward controller term k by a constant.

Appendix C

Memory Requirements and Computational Complexity

Equation (3.14) gives the control law and the adaptation laws. Note that the finite integral term is approximated as shown in (3.22) and together with the λ_i terms introduced by this approximation we have totally 12 controller parameters. These control parameters multiplies the 12 states to form 12 terms that add up to form the control signal. In addition we need 12 terms to update the controller parameters. To calculate the update laws we also need to know the tracking error and 12 adaptation rates, together with z_y for the fine-tuning. For the robustness scheme, we need to store the value of σ and 12 different threshold values. Summing these up, we have totally 85 float variables that needs 340 bytes of memory space.

As for the number of operations, we have 12 multiplication operations to create the terms in the control signal, 11 sums to add up those terms, 36 multiplications for the calculation of the adaptive law terms terms and 12 additions for updating the control parameters and 12 comparisons for the robustness scheme. Totally we have 83 operations per computation cycle. With a 30 ms sampling rate of the idle speed control algorithm, we have approximately $2.8 \cdot 10^3$ flops. Assuming an average ECU speed of 10^7 flops, we need 0.028 percent of the total computational power.

Appendix D

Stability of Integral Approximation

The closed loop system, with the controller using (3.22) as the integral approximation, has an unbounded sequence of characteristic roots whose accumulation points have real parts that are equal to the real parts of the roots of the following equation [75]:

$$u(t) = \lambda_1(t)u(t - dt) + .. + \lambda_m(t)u(t - mdt) \tag{D.1}$$

where $m = 5$. We observed in the experiments that λ_i values were in the order of 10^{-4}. Using this value as the avarage value for λ_i's and taking the Laplace transform of (D.1), we obtain the following characteristic equation:

$$1 - 10^{-4}\left(e^{-0.03s} + .. + e^{-0.15s}\right) = 0 \tag{D.2}$$

It is obvious that the characteristic roots can not have positive real parts. Referring the average value of λ_i's as λ_{avg} and considering the case where the characteristic roots are on the jw axis, so the real parts of the roots are 0, we obtain that

$$1 - \lambda_{\text{avg}}\left(e^{-0.03\text{j}\beta} + .. + e^{-0\ 15\text{j}\beta}\right) = 0 \tag{D.3}$$

where jβ refers to the imaginary part of the characteristic root. Note that for $\beta = 0$, (D.3) is satisfied if $\lambda_{\text{avg}} = 0.2$. Therefore, unless $\lambda_{\text{avg}} \geqslant 0.2$, (D.3) can not be satisfied and hence all the roots remain in the left half complex plane. This means that even

if the observed values of λ_i's were $0.2/10^{-4} = 2000$ times larger, we would still have an integral approximation that would yield a stable closed loop system.

Bibliography

[1] Q.-G. Wang, T. H. Lee, and K. K. Tan, *Finite Spectrum Assignment for Time-Delay Systems*, ser. Lecture Notes in Control and Information Sciences, M. Thoma, Ed. New York: Springer-Verlag, 1999, vol. 239.

[2] V. B. Kolmanovsky and A. Myshkis, *Introduction to the theory and applications of functional differential equations.* Dordrecht: Kluwer Academy, 1999.

[3] S. I. Niculescu, *Delay effects on stability.* Berlin: Springer., 2001.

[4] J.-P. Richard, "Time-delay systems:an overview of some recent advances and open problems," *Automatica*, vol. 39, pp. 1667–1694, 2003.

[5] K. Gu and S.-I. Niculescu, "Survey on recent results in the stability and control of time-delay systems," *Journal of Dynamic Systems, Measurement and Control*, vol. 125, no. 2, pp. 158–165, 2003.

[6] J. Jang, "Adaptive control design with guaranteed margins for nonlinear plants," Ph.D. dissertation, Massachusetts Institute of Technology, 2008.

[7] O. J. Smith, "A controller to overcome dead time," *ISA Journal*, vol. 6, 1959.

[8] K. J. Astrom, C. C. Hang, and B. C. Lim, "A new Smith predictor for controlling a process with an integrator and long dead-time," *IEEE Transactions on Automatic Control*, vol. 39, no. 2, pp. 343–345, Feb. 1994.

[9] S. Majhi and D. Atherton, "A new smith predictor and controller for unstable and integrating processes with time delay," in *Proc. Conference on decision and control*, Tampa, FL, Dec. 1998.

[10] M. Fliess, R. Marquez, and H. Mounier, "PID-like regulators for a class of linear delay systems," in *Proc. Europ. Control Conf.*, Porto, Portugal, Sep. 2001.

[11] Z. J. Palmor, "Time-delay compensation-Smith predictor and its modifications," in *The control handbook*, W. Levine, Ed. Boca Raton, FL, USA: CRSC Press, 1996, pp. 224–237.

[12] A. Z. Manitius and A. W. Olbrot, "Finite spectrum assignement problem for systems with delays," *IEEE Transactions on Automatic Control*, vol. 24, no. 4, 1979.

[13] K. Watanabe, E. Nobuyama, T. Kitamori, and M. Ito, "A new algorithm for finite spectrum assignment of single-inputsystems with time delay," *IEEE Transactions on Automatic Control*, vol. 37, no. 9, pp. 1377–1383, Sep. 1992.

[14] H. Glusing-Luerben, "A behavioral approach to delay-differential systems," *SIAM Journal on Control and Optimization*, vol. 35, no. 2, pp. 480–499, 1997a.

[15] J. J. Loiseau and D. Brethe, "An efective algorithm for finite spectrum assignment of single-input systems with delays," *Mathematics and Computers in Simulation,*, vol. 45, no. 3-4, pp. 339–348, 1998.

[16] K. Ichikawa, "Frequency-domain pole assignement and exact model-matching for delay systems," *International Journal of Control*, vol. 41, pp. 1015–1024, 1985.

[17] R. Ortega and R. Lozano, "Globally stable adaptive controller for systems with delay," *International Journal of Control*, vol. 47, no. 1, pp. 17–23, 1988.

[18] K. S. Narendra and A. M. Annaswamy, *Stable adaptive systems.* New York: Dover Publications, 2005.

[19] S.-I. Niculescu and A. M. Annaswamy, "An adaptive smith-controller for time-delay systems with relative degree $n \leqslant 2$," *Systems and Control Letters*, vol. 49, pp. 347–358, 2003.

[20] L. Guzzella and C. H. Onder, *Introduction to Modeling and Control Internal Combustion Engine Systems*, 1st ed. Springer, 2004.

[21] D. Hrovat and J. Sun, "Models and control methodologies for ic engine idle speed control design," *Control Eng. Practice*, vol. 5, no. 8, pp. 1093–1100, 1997.

[22] S. J. Williams *et al*, "Idle speed control design using an H_∞ approach," in *Proc. Amer. Control Conf.*, 1989, pp. 1950–1956.

[23] R. D. Filippi and R. Scattolini, "Idle speed control of a F1 racing engine," *Control Eng. Practice*, vol. 14, no. 3, pp. 251–257, 2005.

[24] L. Kjergaard, S. Nielsen, T. Vesterholm, and E. Hendricks, "Advanced nonlinear engine idle speed control systems," in *Proc. of SAE*, no. 940974, 1994.

[25] X. Li and S. Yurkovich, "Sliding mode control of delayed systems with application to engine idle speed control," *IEEE Transactions on Control Systems Technology*, vol. 9, no. 6, pp. 802–810, Nov. 2001.

[26] K. R. Butts, N. Sivashankar, and J. Sun, "Application of ℓ_1 optimal control to the engine idle speed control problem," *IEEE Transactions on Control Systems Technology*, vol. 7, no. 2, pp. 258–270, 1999.

[27] T.-L. Chien, C.-C. Chen, and C.-Y. Hsu, "Tracking control of nonlinear automobile idle-speed time-delay system via differential geometry approach," *Journal of the Franklin Institute*, vol. 342, no. 7, pp. 760–775, Nov. 2005.

[28] P. K. Kokotovic and D. Rhode, "Sensitivity guided design of an idle speed controller," Ford Motor Company, PK Research, Urbana, U.S.A., Technical Report 1, 1986.

[29] A. Gangopadhyay and P. Meckl, "Multivariable pi tuning and application to engine idle speed control," in *Proc. Amer. Control Conf.*, San Diego, CA, June 1999, pp. 2678–2682.

[30] J. Grizzle, J. Buckland, and J. Sun, "Idle speed control of a direct injection spark ignition stratified charge engine," *Int. J. Robust Nonlinear Control*, vol. 47, no. 1, pp. 17–23, 1988.

[31] S. Yurkovich and M. Simpson, "Crank-angle domain modeling and control for idle speed," *SAE Paper*, no. 970027, 1997.

[32] Y. Wang, A. Stefanopoulou, and M. Levin, "Idle speed control: An old problem in a new engine design," in *Proc. Amer. Control Conf.*, San Diego, CA, June 1999, pp. 1217–1221.

[33] B. K. Powell and W. F. Powers, "Linear quadratic control design for nonlinear ic engine systems," in *Proc. of ISATA Conference*, Stockholm, Sweden, 1981.

[34] G. D. Nicolao, C. Rossi, R. Scattolini, and M. Suffritti, "Identification and idle speed control of internal combustion engines," *Control Eng. Practice*, vol. 7, no. 9, pp. 1061–1069, Sep. 1999.

[35] D. Hrovat, "MPC-based idle speed control for IC engine," in *Proc. of FISITA conference*, Prague, Czech Rep., 1996.

[36] W. P. Mihelc and R. D. Citron, "An adaptive idle speed mode control design," in *Proc. of SAE*, no. 840443, 1981.

[37] D. Kim and J. Park, "Application of adaptive control to the fluctuation of engine speed at idle," *Information Sciences*, vol. 177, no. 16, pp. 3341–3355, Aug. 2007.

[38] F.-C. Hsieh, B.-C. Chen, and Y.-Y. Wu, "Adaptive idle speed control for spark-ignition engines," *SAE Paper*, no. 2007-01-1197, 2007.

[39] A. Stotsky, B. Egardt, and S. Eriksson, "Variable structure control of engine idle speed with estimation of unmeasurable disturbances," *Journal of Dynamic Systems, Measurement and Control*, vol. 122, no. 4, pp. 599–603, 2000.

[40] D. Pavkovi, J. Deur, V. Ivanovi, and D. Hrovat, "SI engine load torque estimator based on adaptive kalman filter and its application to idle speed control," *SAE Paper*, no. 2005-01-0036, 2005.

[41] S. Niwa and M. Kajitani, "High performance idle speed control applying the disturbance cancellation control," *SAE Paper*, no. 2003-08-0392, 2003.

[42] M. Thornhill, S. Thompson, and H. Sindano, "A comparison of idle speed control schemes," *Control Eng. Practice*, vol. 8, no. 5, pp. 519–530, May 2000.

[43] Y. Yildiz, A. Annaswamy, I. Kolmanovsky, and D. Yanakiev, "Adaptive posicast controller," *Automatica*, submitted. http://web.mit.edu/aaclab/publications/index.html.

[44] M. Shelef and R. W. McCabe, "Twenty-five years after introduction of automotive catalysts: what next?" *Catalysis Today*, vol. 62, no. 1, pp. 35–50, Sep. 2000.

[45] L. Guzzella, "Models and model-based control of IC-engines A nonlinear approach," *SAE Paper*, no. 950844, 1995.

[46] B. Ault, V. K. Jones, J. D. Powell, and G. F. Franklin, "Adaptive air-fuel ratio control of a spark-ignition engine," *SAE Paper*, no. 940373, 1994.

[47] R. Turin and H. Geering, "Model-reference adaptive A/F ratio control in an SI engine based on Kalman-Filtering techniques," in *Proc. Amer. Control Conf.*, 1995, pp. 4082–4090.

[48] V. K. Jones, B. A. Ault, G. F. Franklin, and J. D. Powell, "Identification and air-fuel ratio control of a spark ignition engine," *IEEE Transactions on Control Systems Technology*, vol. 3, no. 1, Mar. 1995.

[49] D. Rupp, C. Onder, and L. Guzzella, "Iterative adaptive air/fuel ratio control," in *Proc. Advances in Automotive Control*, Seascape Resort, USA, 2008.

[50] L. Guzzella, M. Simons, and H. P. Geering, "Feedback linearizing air/fuel-ratio controller," *Control Eng. Practice*, vol. 5, no. 8, pp. 1101–1105, Aug. 1997.

[51] C.-F. Chang, N. P. Fekete, A. Amstutz, and J. D. Powell, "Air-fuel ratio control in spark-ignition engines using estimation theory," *IEEE Transactions on Control Systems Technology*, vol. 3, no. 1, Mar. 1995.

[52] J. D. Powell, N. P. Fekete, and C. F. Chang, "Observer-based air-fuel ratio control," *IEEE Control Systems Magazine*, vol. 18, no. 5, pp. 72–83, Oct. 1998.

[53] S. B. Choi and J. K. Hedrick, "An observer-based controller design method for improving air/fuel characteristics of spark ignition engines," *IEEE Transactions on Control Systems Technology*, vol. 6, no. 3, pp. 325–334, May 1998.

[54] M. Won, S. B. Choi, and J. K. Hedrick, "Air-to-fuel ratio control of spark ignition engines using gaussian network sliding control," *IEEE Transactions on Control Systems Technology*, vol. 6, no. 5, pp. 678–687, Sep. 1998.

[55] J. K. Pieper and R. Mehrotra, "Air/fuel ratio control using sliding mode methods," in *Proc. Amer. Control Conf.*, San Diego, CA, June 1999, pp. 1027–1031.

[56] J. S. Souder and J. K. Hedrick, "Adaptive sliding mode control of air-fuel ratio in internal combustion engines," *Int. J. Robust Nonlin. Cont.*, vol. 14, no. 6, pp. 525–541, Apr. 2004.

[57] A. Ohata, M. Ohashi, M. Nasu, and T. Inoue, "Crank-angle domain modeling and control for idle speed," *SAE Paper*, no. 950075, 1995.

[58] C. H. Onder and H. P. Geering, "Model-based multivariable speed and air-to-fuel ratio control of an si engine," *SAE Paper*, no. 930859, 1993.

[59] C. W. Vigild, K. P. H. Andersen, E. Hendricks, and M. Struwe, "Towards robust H-infinity control of an SI engine's air/fuel ratio," *SAE Paper*, no. 1999-01-0854, 1999.

[60] L. Mianzo, H. Peng, and I. Haskara, "Transient air-fuel ratio H_∞ preview control of a drive-by-wire internal combustion engine," in *Proc. Amer. Control Conf.*, 2001, pp. 2867–2871.

[61] S. Nakagawa, K. Katogi, and M. Oosuga, "A new air-fuel ratio feedback control for ulev/sulev standard," *SAE Paper*, no. 2002-01-0194, 2002.

[62] Y.-J. Zhai and D.-L. Yu, "Neural network model-based automotive engine air/fuel ratio control and robustness evaluation," *Engineering Applications of Artificial Intelligence*, in press.

[63] K. R. Muske and C. P. J. Jones, "A model-based si engine air fuel ratio controller," in *Proc. Amer. Control Conf.*, 2006, pp. 3284–3289.

[64] C. F. Chang, N. P. Fekete, and J. D. Powell, "Engine air-fuel ratio control using an event-based observer," in *Proc. of SAE*, no. 930766, 1993.

[65] A. G. Stefanopoulou, J. W. Grizzle, and J. S. Freudenberg, "Engine air-fuel ratio and torque control using secondary throttles," in *Proc. of Conference on Decision and Control*, 1994, pp. 2748–2753.

[66] Z. F., K. Grigoriadis, M. Franchek, and I. Makki, "Linear parameter varying lean burn air-fuel ratio control for a spark ignition engine," *Journal of Dynamic Systems, Measurement and Control*, vol. 129, pp. 404–414, 2007.

[67] P. Tunestal and J. K. Hedrick, "Cylinder air/fuel ratio estimation using net heat release data," *Control Eng. Practice*, vol. 11, no. 3, pp. 311–318, Mar. 2003.

[68] I. Arsie, C. Pianese, G. Rizzo, and V. Cioffi, "An adaptive estimator of fuel film dynamics in the intake port of a spark ignition engine," *Control Eng. Practice*, vol. 11, no. 3, pp. 303–309, Mar. 2003.

[69] L. Mirkin and N. Raskin, "Every stabilizing dead-time controller has an observer-predictor-based structure," *Automatica*, vol. 39, no. 10, pp. 1747–1754, 2003.

[70] L. Debnath and P. Mikusinski, *Introduction to Hilbert Spaces with Applications*, 3rd ed. Elsevier, 2005.

[71] W. Rudin, *Principles of Mathematical Analysis*, 3rd ed., A. A. Arthur and S. L. Langman, Eds. New York: McGraw-Hill, Inc., 1976.

[72] K. S. Narendra, A. M. Annaswamy, and R. P. Singh, "A general approach to the stability analysis of adaptive systems," *International Journal of Control*, vol. 41, no. 1, pp. 193–216, 1985.

[73] M. Krstic, "On compensating long actuator delays in nonlinear control," *IEEE Transactions on Automatic Control*, vol. 53, no. 7, pp. 1684–1688, 2008.

[74] K. S. Narendra and A. M. Annaswamy, *Stable Adaptive Systems.* Englewood Cliffs, NJ: Prentice-Hall, 1989.

[75] K. Engelborghs, M. Dambrine, and D. Roose, "Limitations of a class of stabilization methods for delay systems," *IEEE Trans. Automatic Control*, vol. 46, no. 2, Feb. 2001.

[76] S. P. Karason and A. M. Annaswamy, "Adaptive control in the presence of input constraints," *IEEE Trans. Automatic Control*, vol. 39, no. 11, pp. 2325–2330, Nov. 1994.

[77] M. J. van Nieuwstadt, I. V. Kolmanovsky, P. E. Moraal, A. Stefanopoulou, and M. Jankovic, "EGR-VGT control schemes: experimental comparison for a high-speed diesel engine," *IEEE Control Systems Magazine*, vol. 20, no. 3, pp. 63–79, Jun. 2000.

[78] S. Majhi and D. P. Atherton, "Obtaining controller parameters for a new Smith predictor using autotuning," *Automatica*, vol. 36, no. 11, pp. 1651–1658, Nov. 2000.

[79] Y. Yildiz, A. Annaswamy, D. Yanakiev, and I. Kolmanovsky, "Spark ignition engine idle speed control: An adaptive control approach," *IEEE Transactions on Control Systems Technology*, submitted. http://web.mit.edu/aaclab/publications/index.html.